UNIVERSITY OF CALIFORNIA, SAN DIEGO

In Vivo Tibial Force Measurement After Total Knee Arthroplasty

A Dissertation submitted in partial satisfaction of the requirements for the degree

Doctor of Philosophy

in

Bioengineering

by

Darryl David D'Lima

Committee in charge:

Professor Shu Chien, Chair
Professor Michael Berns
Professor Alan Hargens
Professor Michael Heller
Professor Pin Tong

2007

This Dissertation of Darryl David D'Lima is approved, and it is acceptable in quality and form for publication on microfilm:

_____

_____

_____

_____

_____
Chair

University of California, San Diego

2007

DEDICATION

This dissertation is dedicated to my mother, Celine D'Lima, who saw the scientist in me and instilled the spirit of life-long learning; to my father, Gerald D'Lima, who always found the best in everyone; to my wonderful wife, Amy, who managed a full-time job and kept the family together; and to my son, David, and daughter, Dominique, who continue to show me new ways to enjoy life.

TABLE OF CONTENTS

LIST OF FIGURES

LIST OF TABLES

ACKNOWLEDGEMENT

I would like to thank Professor Shu Chien for his unfailing support and encouragement and his invaluable assistance in drafting this dissertation. This research would not have been possible without the vision and dedication demonstrated by Dr. Clifford W. Colwell Jr, the surgeon who directed the design and development of the electronic knee and performed the surgical implantation. I would like to thank Peter Chen, Nikolai Steklov, Shantanu Patil, Juan Hermida, Zachary Dooley for their valuable assistance in conducting the experiments and in data collection. I am indebted to Scott Banks, PhD, and BJ Fregly PhD for collecting and analyzing the fluoroscopic data. I am also grateful for Judy Blake's help in the formatting, copyediting, and proofing of this dissertation.

The contents of Chapter 3 have been published in the Journal of Biomechanics: D. D'Lima, S. Patil, N. Steklov, S. Chien, C. Colwell Jr. In vivo knee moments and shear after total knee arthroplasty. Journal of Biomechanics, Volume 40, Pages S11-S17, 2007

VITA

1982	MBBS, Bombay University, India
1983 – 1987	Orthopaedic Surgery Residency, Bombay University, India
1987	Master of Surgery, Bombay University, India
2005	Master of Science, University of California, San Diego
2007	Doctor of Philosophy, University of California, San Diego

ABSTRACT OF THE DISSERTATION

In Vivo Tibial Force Measurement After Total Knee Arthroplasty

by

Darryl David D'Lima

Doctor of Philosophy in Bioengineering

University of California, San Diego, 2007

Professor Shu Chien, Chair

Knee forces after total knee replacement are directly related to the transmission of stresses including contact stresses generated at the bearing surface, stresses at the implant-cement-bone interface and stresses transmitted to underlying bone. These stresses are a major factor in wear and fatigue, aseptic loosening and implant migration, bone remodeling, stress shielding and osteoporosis, all of which determine the life of the implant. We report for the first time the in vivo measurement of tibial forces, shear and moments. A custom telemetry-enabled implantable device

was used to measure tibiofemoral forces in vivo. We implanted the telemetry-based device into three patients scheduled for total knee arthroplasty. We measured knee forces and kinematics during activities of daily living. The axial component of forces predominated, especially during the stance phase of the activities studied. During walking, forces peaked between 2 and 3 x body weight. Peak tibial forces were substantially higher while climbing stairs (averaging 3 x body weight) than for the chair-rise and squat activities. Overall, shear forces, as well as moments at the tibial tray, were fairly low. We report on the first finite element model of knee joint arthroplasty using in vivo knee forces for the calculation of polyethylene stresses. Walking and stair-climbing generated peak contact stresses below the threshold that is generally considered safe for polyethylene. Contact stresses generated during high flexion activities were substantially higher and largely due to the reduced contact area in deep flexion rather than an increase in contact forces. These results support the use of “high-flexion” designs that improve contact conditions and preserve contact area at high flexion angles. These data can be used to validate existing models of the knee that estimate these forces and to develop more accurate models. Knowledge of in vivo forces can be used to design more effective in vitro knee testing rigs and knee wear simulators that can accurately model knee function and prosthetic wear. Finally, these results can directly enhance prosthetic design.

Chapter 1

Introduction

1.A Total Knee Arthroplasty

Total knee arthroplasty is an effective surgery that relieves pain and restores function after end-stage arthritis of the knee (Fig 1). Over two hundred thousand knee joints are surgically replaced worldwide every year [98,99] with the number expected to double by the year 2030 due to the increase in population and the increase in life expectancy.[1,132] With prolonged life expectancy and rising number of arthroplasties being performed in younger patients, longer survival is essential. Increasing long-term successes have been reported with several contemporary total knee replacement designs lasting up to and over 15 years.[2,19,48,95,136] However, despite the overall high survival, 22,000 knee arthroplasties were revised in 1999 and the number of revisions is expected to increase substantially.[37] Earlier reports of revision arthroplasty implicated infection as the primary cause for failure.[22,49,109] However, more recent reports ranked polyethylene wear the highest (25% of all failures), followed by aseptic loosening (24%), and instability (21%).[120]

Survival and function of knee implants is dependent on several interrelated parameters, which makes it difficult to predict the effect of design changes. In vitro experiments and mathematical models have the advantage of being safer, better controlled and precise, and are used as cost- and time-effective screening tools before clinical evaluation.[47,57,96,105,122,141] Tibial forces along with the kinematic patterns of the knee have a significant effect on the type and quantity of wear

produced.[16,30] Hence, tibiofemoral force measurements are extremely valuable in gaining insight in vivo conditions and in developing predictive models.

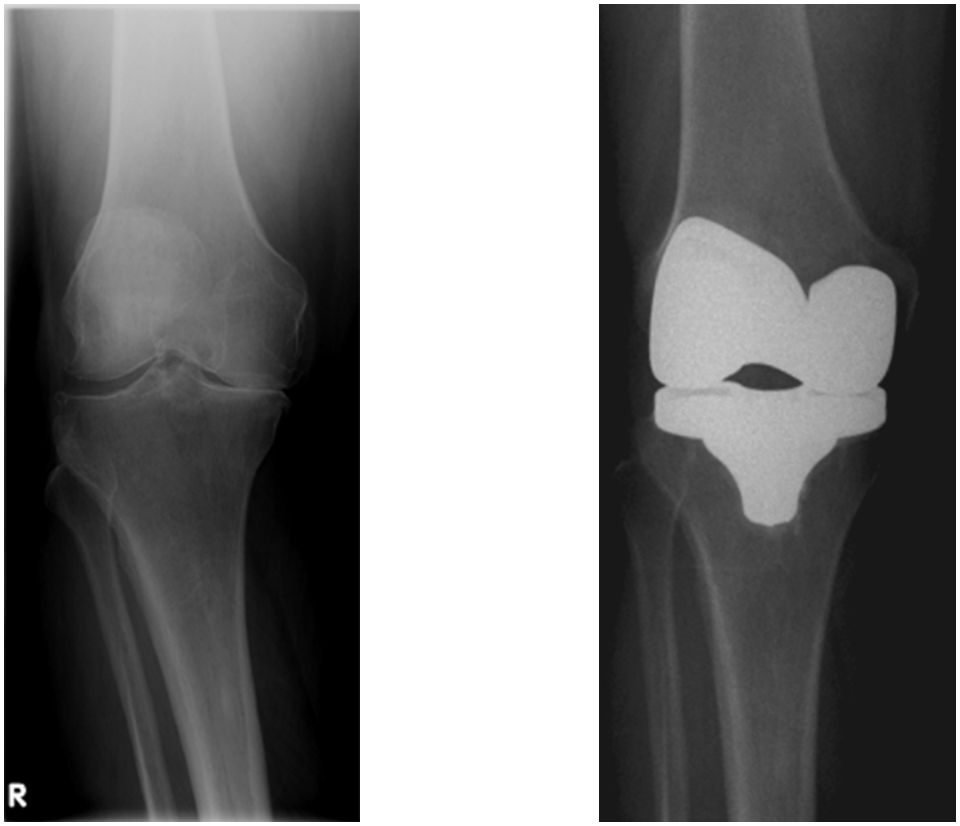

Figure 1: Radiograph of a total knee arthroplasty. **Left:** Radiograph of severe knee osteoarthritis with varus deformity. **Right:** Postoperative radiograph of the same knee after replacement with prosthetic components and correction of deformity.

1.B Polyethylene Contact Stresses and Wear

Increasing long-term successes have been reported with several contemporary total knee replacement designs.[2,19,40,48,95,136] As a result, wear-related phenomena have become the most common reason for revision. [5,20,23,41,75,84,92,92,137] Some have reported wear even in short-term follow-up studies[5,84,92] ranging from 10% to 50% of arthroplasty patients presenting symptoms or requiring revision surgery.[41,75] A few studies have reported a failure rate due to wear as high as 7% at an average of less than 5 years[131] and osteolytic rates of 8% in cemented compared with 16% in noncemented knee arthroplasties.[2,104] Excessive polyethylene wear has been reported at less than 10-year follow up and has been attributed to heat-pressed surfaces, implant design, subsurface damage, malalignment and instability.[15,24,43,63,66,72,92,133] To address the potential for wear, several design changes,[107,130,141] manufacturing processes,[90,140] and alternative bearing surfaces[65,78,117] are being developed. Clinical evaluation of these measures typically involves several years of postoperative follow up and can expose patients to potential risk. In vitro wear simulation is valuable as a safe, cost- and time-efficient method of determining long-term polyethylene wear.

Contact stresses can often exceed the yield strength of ultra high molecular weight polyethylene.[10,62,80,125]. The reported average contact area of a natural knee joint ranges from 765 to 1150 mm^2, which drops to between 80 and 300 mm^2 after total knee arthroplasty depending on the design and on load conditions.[53,71,106,108] Contact stresses on the insert may therefore rise to as high as 30 to 60 MPa.[80,125] This significantly exceeds the yield point of polyethylene (15–20 MPa).[79] Tibial forces along with the kinematic patterns of the knee have been shown to have a significant

effect on the type and quantity of wear produced.[16,30] Hence, valid tibiofemoral force values are essential to reproduce in vivo conditions accurately and to develop predictive models.

1.C Estimation of Tibial Forces

Several studies have attempted to estimate forces at the knee during various activities. These reports have utilized various approaches incorporating static or dynamic analysis, forward or inverse dynamics, 2-dimensional or 3-dimensional analysis, and the inclusion or exclusion of muscle forces. One report studied knee forces in open and closed kinetic chain knee extension and estimated knee forces to be approximately 5 times body weight.[87] Similarly, another study of 2-dimensional isokinetic model of knee flexion/extension estimated peak tibiofemoral compressive forces up to 5 times body weight.[100] On the other hand, when inertial effects and muscle activation (from EMG data and linear optimization methods) were included, the predicted knee forces dropped to 4 times body weight for the same activity.[69]

Co-contraction of antagonistic muscles (such as hamstring and quadriceps muscle co-contraction during a squat) can also affect knee forces.[83,138] A major difficulty in solving for muscle forces when using inverse dynamics is the indeterminate nature of the problem, since more than one muscle may be contracting at a given time. One approach has been to reduce this redundancy by grouping muscles with similar function and by rejecting inappropriate solutions.[26,101] An alternate approach has been to optimize the solution using various criteria such as minimizing total muscle force or instantaneous muscle power.[28,69,83,119] However, predicted forces were substantially different when different approaches to estimate muscle forces were used.[82,102]

The knee is a complex joint that is difficult to model accurately. Although significant advances have been made in mathematical modeling, these have yet to be conclusively validated in vivo. All the above-mentioned studies make several assumptions that have yet to be substantiated. A recent report predicted knee forces in four patients (implanted with instrumented hip prostheses) that were substantially higher than those measured in the first patient we implanted with an instrumented knee prosthesis.[128] Direct in vivo measurement of tibial compressive forces provides an invaluable means of validating such models. An accurate, clinically applicable model is extremely valuable and can be used for evaluating the effect of design changes, assessing different surgical techniques and component alignment, and for designing and developing in vitro knee wear simulation protocols.

1.D Measurement of Tibial Forces

Tibial forces have been measured in vitro as early as 1975 using a tibial plate connected to an instrumented shaft by Perry et al.[103] Singerman et al reported on a force-transducer design based on two concentric cylinders. The inner cylinder was instrumented with strain gages while the outer cylinder was fixed to bone.[121] This transducer was used to measure tibial forces in normal cadaver knees and was inserted through a 1-cm resection of proximal tibial. Kaufman et al[70] reported on a tibial prosthesis instrumented with load cells that could measure the magnitude of axial compressive force on the tibia in vitro. Accuracy testing demonstrated a correlation of 0.999 between the actual and calculated load. When calculating the location of the applied load, the error was a 0.07 ± 0.41 mm in the mediolateral direction and 0.24 ± 0.34 mm in the anteroposterior direction. The same instrumented prosthesis was subsequently used in cadaver studies which measured

the effect of joint-line elevation on tibiofemoral forces after total knee arthroplasty.[57] We have also presented the results of testing a prototype telemetry tibial replacement system, using radiofrequency transmission (RF) of data, which demonstrated comparable accuracy in measuring the tibiofemoral compressive forces and location.[35] This telemetry system was found to transmit the signal through bone, cement, and soft tissues accurately within a range of approximately 3 meters. In addition, the system also worked intraoperatively.[93] These studies establish the accuracy and reliability of this method of measuring tibial forces.

1.E Telemetry in Orthopaedics

Rydell [115] was the first to measure hip forces in vivo with an instrumented Austin-Moore prosthesis using direct-wired connections to subcutaneous leads. Subsequently, in vivo forces have been successfully measured in orthopaedics in the hip,[12-14,17,38,58,59,61,76,77] spine,[21,113,139] and femur[85,86,126,127] using telemetry links. The first report of a telemetered hip prosthesis came from English and Kilvington, who reported hip forces of 2.7 times body weight during the stance phase of level walking without support.[44] Davy et al[39] implanted a femoral prosthesis with a triaxial load cell and measured peak hip forces of 2.6 times body weight during both level walking and stair-climbing. This was significantly less than the reports of hip force estimates that ranged from 3.3 to 6.9 times body weight.[39] Subsequent reports of in vivo hip forces have been fairly consistent: 2.7 times body weight for walking at a normal pace,[77] 2.8 to 4.8 times body weight for walking at faster speeds, 2.5 to 5.5 times body weight for jogging and slow jumping.[12,13] In a controlled comparison, Brand et al reported that calculated peak hip forces were consistently higher (by 0.5 times body weight) than those measured in the same patient.[17]

Lu et al[86] measured femoral shaft axial forces in a massive proximal femoral replacement prosthesis. A significant increase in the ratio of measured forces to externally applied force was found ranging from 1.3 in double leg stance to more than 20 during isometric contraction. This demonstrates that muscle contraction contributes a significant component of the actual force generated in the shaft of the femur as opposed to that calculated from external forces alone. Therefore, appropriate simulation of muscle forces is necessary to calculate forces acting on bones and joints. More recently, instrumented distal femoral prostheses have been used to measure forces in the femoral shaft and to estimate tibial forces. The prosthesis used was a distal-femoral replacement for the treatment of bone tumors.[127] The reported peak femoral-axial shaft forces were in the 2.2 to 2.5 times body weight range and the estimated tibial-axial compressive forces were similar. However, the knee prosthesis used was a rotating-hinge design and both heads of the gastrocnemius had been dissected free of the femur; and therefore, these results may not apply to a typical primary total knee arthroplasty.

These studies reveal a significant disparity between typically reported estimates of forces in the hip and the femur and direct measurements in vivo. The knee is much more complex and difficult to model than the hip because of the six degrees of freedom, complex surface geometry, tricompartmental contact, and the fact that stability is largely provided by soft tissues. Direct in vivo measurement of knee forces is therefore essential, if reasonable validation is to be expected.

1.F Overall Objective

This dissertation reports on a custom telemetry-based implantable device to measure tibiofemoral forces in vivo. This device can directly measure forces during activities of daily living (walking, stair-climbing, chair rise). This device can be used to validate existing models of the knee that estimate these forces and to develop more accurate models. Such models provide valuable information that may lead to knee arthroplasty design changes that can improve the function and longevity of total knee prostheses. In conjunction with measured knee motion data, accurate knee force data may also be used to design more effective in vitro knee testing rigs and knee wear simulators that can accurately model knee function and prosthetic wear. Additional uses of this device may be intraoperative measurement of forces to determine soft-tissue balancing, evaluation of the effects of rehabilitation, external bracing, and activities more vigorous than those of daily living (such as athletic and recreational activities).

Knee forces were measured in vivo during activities of daily living and a model was developed to predict risks for polyethylene damage under the following aims.

Aim 1: Implant the telemetry-based device into three patients scheduled for total knee arthroplasty. The implantation of this device will allow the first documented in vivo measurement of internal knee forces and moments. This device will directly measure forces during activities of daily living, and recreational and athletic activities. It can be used to validate existing models of the knee that estimate these forces and to develop more accurate models. Such models provide valuable information that may lead to design changes that can improve the function and longevity of total knee prostheses. In conjunction with kinematic measurements,

experimental tibiofemoral force data may also be used to design more effective knee testing rigs and wear simulators that can accurately model knee function and prosthetic wear.

Aim 2: Measure knee forces and kinematics during activities of daily living. In this aim, tibial forces will be recorded in conjunction with motion analysis during the most common daily living activities to which the knee is subjected. We used a second-generation instrumented tibial prosthesis to measure tibial forces in vivo as well as to validate the data we previously collected using the first-generation device (see Chapter 2 for details regarding the instrumented tibial devices). Typically knee arthroplasty patients are able to return to activities of daily living with minimal residual disability by 6 months after surgery. Wear or fatigue testing of total knee components is usually conducted in vitro under conditions simulating walking. However, tibial forces applied in vitro are based on predictions made by computational models of the knee. These predictions range from 2 to 7 times body weight depending on the type of model used and the assumptions made.[26,42,82,83,87,100,119,138] No in vivo data exist to validate these models. In addition, other activities of daily living such as climbing stairs or kneeling have not been simulated during fatigue testing of total knee components. This is largely due to the lack of convincing data for applying appropriate loads at the knee. Therefore directly measuring tibial force data will be very valuable to the scientific community (investigators engaged in biomechanical modeling of the knee) as well as to the medical device industry (in the design and testing of artificial knee prosthesis).

Aim 3: Construct a finite element model of knee joint arthroplasty for the calculation of in vivo stresses using experimental data. Stresses at the

bearing surface are a major factor in polyethylene wear and fatigue and affect the life of the implant. However, because of the complex geometry of the articular contact and the nonlinear behavior of the polyethylene bearing material, calculation of stresses is not easy. Finite element analysis can be an experimentally validated method for computing contact stresses in knee implants. Given an realistic material model for polyethylene and appropriate boundary conditions, this approach can accurately predict contact stresses. In the knee, contact stresses have been calculated using the finite element method. However, the tibial forces used to predict contact stresses in published reports have been limited to mathematical estimates due to lack of in vivo measurements.[29,46,60,116] Tibial forces and knee kinematics directly measured in vivo will be therefore be used to calculate contact stresses for activities of daily living. In Specific Aim 2 we validated the data collected from the first-generation device. In this aim we used the data from the first-generation device to report contact stresses using in vivo data from the first time. These contact areas and specific stress patterns are valuable and can be used to develop designs that better tolerate extreme stresses.

Chapter 2

Measurement of Tibial Forces In Vivo

2.A First Generation Instrumented Tibial Prosthesis

Our first attempt at designing an instrumented tibial prosthesis was reasonably successful.[36] The first-generation device consisted of four load transducers in the tibial tray (Fig 2 – 3). By measuring the force on each load cell, the total axial load and the location of center of pressure could be determined. In addition, the distribution of forces between the medial and the lateral compartments could be calculated. Figure 3 displays a cross-sectional diagram demonstrating the location of the multi-channel transmitter and the hermetic feed-through antenna. The stem of the implant contained a microtransmitter that received the analog signal through leads from the load cells. The microprocessor filtered and performed analog-to-digital signal conversion and transmitted the data using pulse-code-modulated (PCM) RF signal. Since RF signals do not pass through a sealed titanium shell, a single-pin hermetic feed-through medical grade transmitting antenna was welded at the distal tip of the stem and connected to the microtransmitter. The external receiving antenna captured the transmitted RF signal and generated RS-232 signals, which were directly read using custom software on a PC. Powering the implantable system was challenging. Since batteries contain toxic chemicals, have a limited lifespan, and occupy valuable space, we elected to use remote powering using magnetic near-field coupling. Approximately 40 milliwatts of power could be generated continuously in the internal coil, which was adequate to power the telemetry system. The details of design features of the microtransmitter, the antenna, the receiver, and the remote

powering system have already been reported.[36] In 2004 we implanted the first total knee arthroplasty patient with this prosthesis and recorded forces in the knee for the first time in vivo.[34]

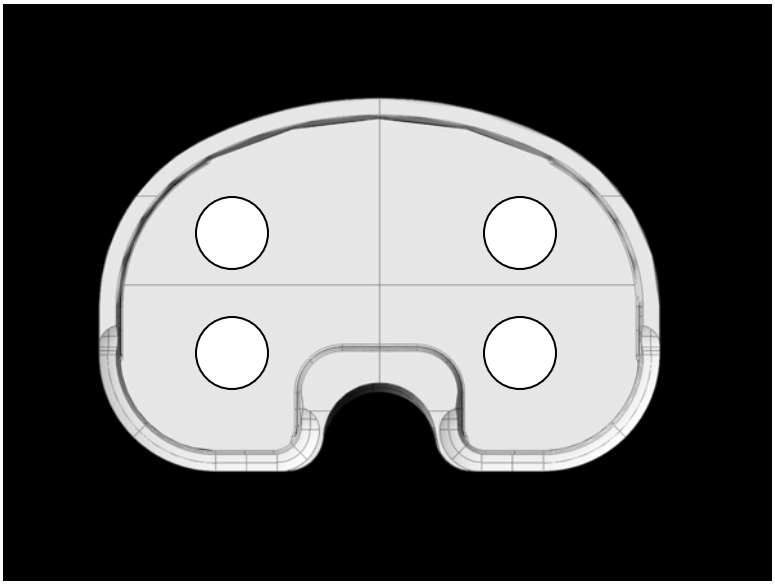

Figure 2A: Top view of the tibial tray: the first generation device had four load cells, one each in each quadrant of the tibial tray. Circles mark the location of the four load cells.

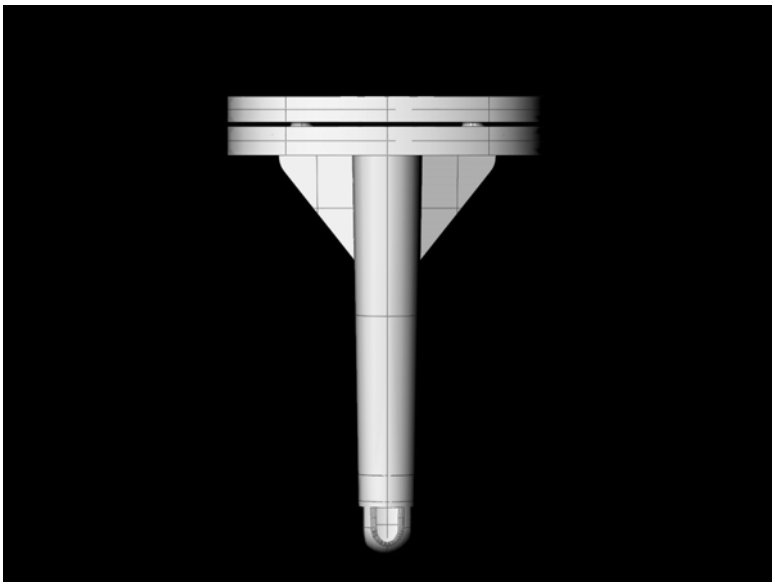

Figure 2B: Anterior view of the implant showing split tibial tray and the polyethylene cap on the end of the stem (protecting the transmitting antenna).

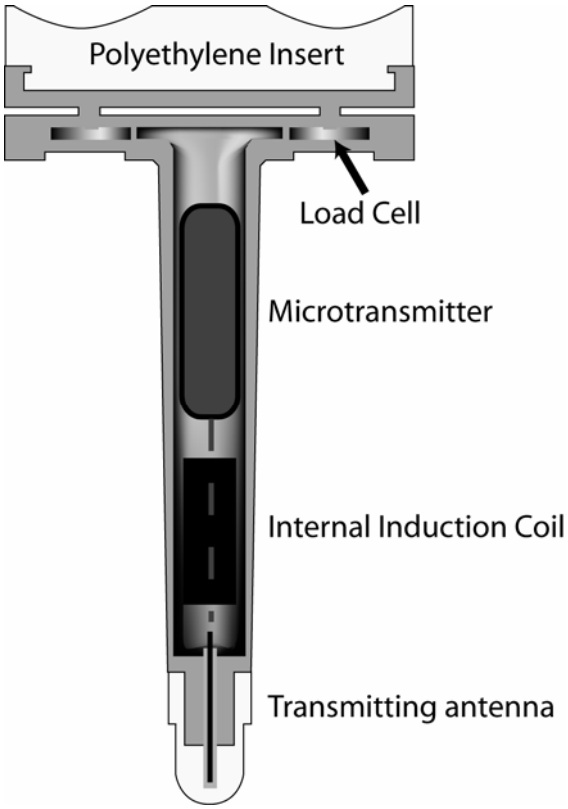

Figure 3: Cross-sectional diagram of the first generation device showing the location of the microtransmitter, internal power induction coil, and transmitting antenna.

2.B Second-Generation Instrumented Tibial Prosthesis

The first-generation electronic knee prosthesis had one major disadvantage: only axial tibial compressive forces were recorded. Shear in the anteroposterior and mediolateral directions and varus/valgus and axial moments are also clinically important components of knee forces. In collaboration with Zimmer, Inc. (Warsaw, IN), we developed a second-generation device to measure all six components of tibial forces (three forces and thee moments).

The design was based on a commercially available tibial tray, polyethylene insert, and instrumentation. The tibial prosthesis was an assembly of two structural components (Fig 4). The proximal section (holding the polyethylene insert) was connected to the distal section (cemented in the tibia) through a cylindrical shrink-fit. The proximal section served as the sensing element and was instrumented with strain gages that measured stem deformation under load. A microprocessor was used to acquire, multiplex, and transmit the data via an RF transmitter and an antenna.

The proximal section (Fig 4B) consisted of the tibial tray and a load-sensing component. A conventional tibial-tray design (NK-II, Zimmer) connected to a hollow stem was machined out of titanium alloy as a single piece (Ti6Al4V). The tibial tray contained the standard locking mechanism for holding a standard polyethylene insert. The inner surface of the hollow stem, which also housed the microtransmitter, was instrumented with 12 strain gages. The tibial tray was proximally unconstrained. The distal portion of the strain-gaged stem was inserted via a thermal shrink-fit into the distal section.

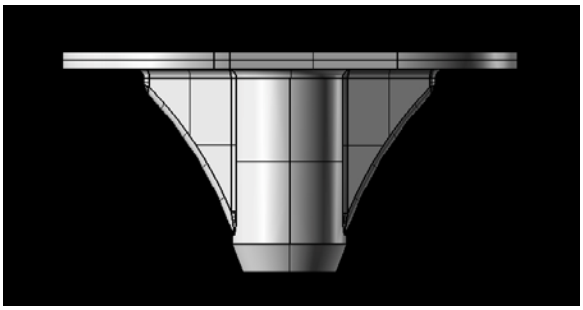

Figure 4A: The second generation device consisted of two components that were assembled via a thermal shrink-fit. Shown here is the distal section.

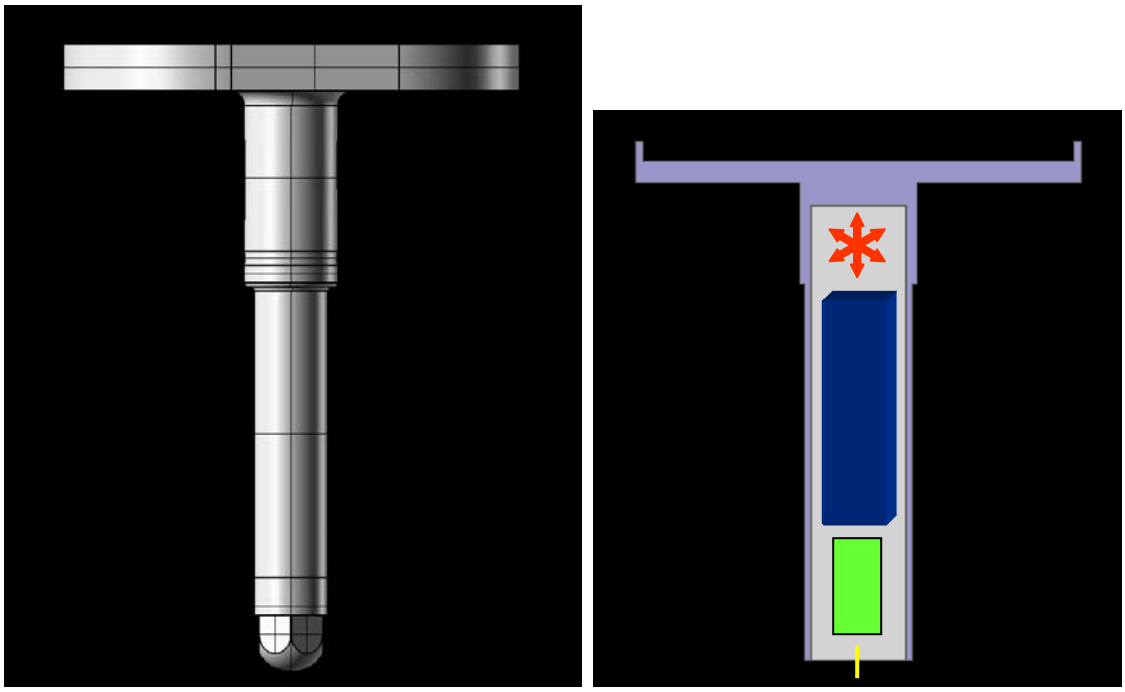

Figure 4B: Left: Rendered image of the stem; **Right:** Cross-sectional diagram. The stem of the proximal section was instrumented with strain gages (red) that measured strain under load and contained the telemetry system (blue) and internal coil (green) and antenna (yellow).

The distal section (shell, Fig 4A) was comprised of a flat platform and a hollow shoulder, which was cemented in the tibia. Knee force transmission was from the femoral-articular surface, through the polyethylene insert, to the tibial tray of the proximal section, and to the distal shell (via the shrink-fit interface). Strains measured

in the strain-gaged stem (connected at one end to the shell and at the other end to the unconstrained tray) were used to compute the net forces acting on the device.

The tibial tray was unconstrained due to a gap (width = 0.635 mm) between the tibial tray and the shell. This gap was chosen as adequate for measuring mediolateral and anteroposterior moments without closure, while allowing for closure of the gap and for protection of the strain gages against overload. The inner diameter of the stem was 16 mm, as this was the minimum diameter required to house the prototype microtransmitter. The minimum thickness of the stem wall was estimated to be 2 mm (resultant outer diameter = 20 mm), which can theoretically withstand fatigue due to 10 million cycles of a bending moment of 20 N-m (assuming a fatigue stress for Ti4Al6V = 396 MPa).

The proximal tray-stem and distal shell were assembled using a thermal shrink-fit between the hollow strain-gaged stem and the shoulder of the shell. Using a coefficient of thermal expansion of 6.39 x 10^{-6}/°C for the titanium alloy[56] and the above nominal inner and outer diameters for the stem, a temperature differential of 6.34°C per micron of expansion was needed. This yielded a minimum temperature differential of 306°C for a nominal shrink-fit interference of 0.05 mm. In actuality, a temperature differential of approximately 700°C was used. The shell was heated in an oven to approximately 500°C, and the stem was cooled to –195°C (in liquid nitrogen). The shell and stem were assembled and were clamped together till temperature equilibrium was achieved and the shrink-fit was stable.

A combination of analytic solutions supported by linear finite-element analysis was used to optimize placement of the strain gages. Three-element stacked-rosette 1000-Ohm strain gages (4 rosettes, total 12 gages, Vishay Micro-Measurements,

Malvern, PA) were bonded to the inner surface of the stem using transducer-grade epoxy. Each rosette was made of three gages: one oriented along the vertical Z-axis, one oriented at -45° to the Z-axis and the other at +45° to the Z-axis. One rosette each was bonded at the anterior, posterior, medial, and lateral surfaces, 16 mm below the bottom of the tibial tray (midway between top of the hollow stem and the most proximal level of the shrink-fit between the tray and the shell). Custom fixtures were used during the procedure to ensure gage location, orientation, and bonding pressure.

Voltage output from the twelve 1000-Ohm resistive strain gages were multiplexed into an instrumentation amplifier. The output of the instrumentation amplifier was digitized by a 12-bit analog-to-digital converter (ADC). Multiple digital samples were digitally filtered by the onboard microprocessor (PIC16f876, Microchip Technology, Chandler, AZ). The microprocessor then serially modulated a 418 MHz frequency shift-keyed radio transmitter (pulse-code modulation) with the digital data. A short radio antenna was attached to a hermetically sealed feed-through to allow for high-frequency transmission out of the subject. A polyethylene cap was added to protect the antenna from damage during the implantation process. Each data packet consisted of a header byte, twelve channels of sensor data (2 bytes each), power-level data (2 bytes), and a checksum (sum of preceding bytes, 2 bytes in size). The header byte was used as a flag for reading the start of the data packet, the checksum byte was used to check the integrity of the data and to test for missing bytes. The PCM receiver contained a receiving antenna, a matched RF oscillator, and a level converter to generate RS-232 signals from the incoming PCM data stream. Custom PC-based software was developed to read, display, and store received data. A PC

received the RS-232 signal, which was read by custom software and was synchronized with data from other instruments.

The microtransmitter was powered using magnetic near-field coupling. An external coil (driven with AC current) generated an AC voltage in the internal coil. This voltage was then rectified and filtered to provide the DC power required to operate the telemetry system. A function generator was used to provide a 3-V AC signal at 1.6 kHz to a 100-W audio-power amplifier, which amplified the signal and drove the external (primary) coil. The power amplifier delivered 1.0 Amps of current at 35 V to the external coil. An external coil of 17 cm in diameter was chosen to allow it to be placed around the patient's leg. The external coil was constructed of 35 turns of 16-gauge magnet wire, with an impedance of 10 Ohms at the 1.6 kHz frequency. The internal (secondary) coil, housed in the stem of the implant, consisted of 2000 turns of magnet wire wound on a high-permeability ferrite core. In this configuration, the internal coil consistently generated approximately 40 milliwatts of power, which was more than adequate to power the strain gages and the telemetry system. Data were collected in both wired and wireless mode and were compared for integrity. Less than 2% of the data was flagged with errors in the checksum byte. Of the data that passed the checksum test, a 100% match was obtained between the wired and wireless recordings.

2.C Calibration and PreClinical Testing

Calibration: The device was secured in a mounting fixture that was aligned with the axis of a six-degree of freedom load cell (AMTI, Watertown, MA), which served as the measurement standard. Individual components of force were separately applied to the surface of the tray. For each applied force continuous data

were synchronously logged from the measurement standard and the strain gages. The offset between the location of the measurement standard and the surface of the tray was used to transform forces and moment output from the measurement standard to yield forces and torques at the tray surface.

One set of loads was used to determine the calibration matrix, while a different set was used to measure error. Calibration loads were selected in the range of –600 to +4000 N for Fz (vertical load), and –600 to +600 N for Fx, and Fz (anteroposterior and mediolateral loads respectively). Moments were selected in the range of –25 to +25 N-m. Multiple linear regressions (one per force component) were used to relate the 12 simultaneous strain measurements to each component of force. Additionally, the error between the forces predicted by strain-gage measurement and those recorded by the measurement standard were calculated. To determine the accuracy under dynamic conditions, measurements were made using a sinusoidal loading waveform at varying frequencies up to 2 Hz.

A highly linear response ($R^2 > 0.997$) was noted between measured and predicted forces. After calibration, a dynamic force was applied and strains were measured. A very close agreement between the measured and predicted forces was found. The experimental determination of the calibration matrix effectively minimized errors in locating or aligning the strain gages, accounted for cross talk between various force components, and automatically weighted the contribution of each strain gage to calculate each component of applied load. After static calibration, the dynamic response of the strain gages was compared with that of the external load cell. To test the value of redundant strain gages, in the event of a failure of a single strain gage, the contributions of each of the 12 gages were individually removed from

the calibration matrix and predicted forces compared with measured forces. Loss of a single strain gage degraded the accuracy by less than 2%.

Under static (unloaded conditions) the telemetry system was tested up to 12 hours duration at a time. The electronics were also subjected to high temperature "burn in" and shaker tests (10 Hz) to determine failure due to fatigue. To test the integrity of the telemetry system, a fresh-frozen cadaveric knee specimen was thawed and a total knee replacement performed. The instrumented tibial prosthesis was cemented into the tibia. The knee was then mounted on a dynamic quadriceps-driven (closed kinetic chain) knee extension rig and tibial forces measured. Forces were initially measured using the prosthesis in a fully wired configuration and again through the telemetry system. The number of checksum errors was used to determine the stability of the telemetry signal during dynamic loading knee motion.

Structural Testing: Six components (tibial trays with stems) were mounted on a fixture designed for cantilever testing on Shore Western Fatigue Frames (Shore Western, Monrovia, CA). The components were fatigue tested in air at room temperature in accordance with ASTM standards [6]. The lateral half of the tray was rigidly clamped while the unsupported medial half was loaded. A cyclic load of 667.5 N was applied in the form of a sinusoidal waveform at 15 Hz for 10 million cycles. All six of the tested specimens survived 10 million cycles at the maximum applied fatigue load without failure or fracture. The surface of each tray was inspected visually and microscopically for signs of fatigue and cracks but none were found.

Strength of the Shrink-fit: Four shells were heated in an oven to approximately 500°C. Four stems were cooled in liquid nitrogen to –195°C. Each stem-shell pair was assembled and clamped together till temperature equilibrium and

stable shrink-fit was achieved . Each stem-shell assembly was mounted on a MTS Bionix testing machine and peak resistance to axial torque was measured at 0.13 deg/sec. Standard NK-II cruciate-retaining femoral components were also tested against corresponding modular inserts in off-the-shelf tibial trays. An axial load of 2670 N was applied across the femorotibial articulation. The maximum torque resistance at the femorotibial articulation (between the femoral component and polyethylene insert) was measured. The maximum torque resistance at the shrink-fit (60 to 85 N-m) was higher than the maximum torque resistance at the femorotibial articulation (16 to 24 N-m).

2.D Surgical Implantation

Patient selection and consent: Institutional review board (IRB) approval at Scripps Clinic was obtained for the clinical study. Otherwise healthy male or female adults, with monoarticular disease of either knee necessitating primary total knee arthroplasty, were screened. Criteria for inclusion were age between 65 and 85 years, and weight between 66 kg and 86 kg (approximately 145 lbs and 190 lbs, respectively). These represent the median range (± one quartile) of the age and weight of the primary total knee arthroplasty population at Scripps Clinic. Other criteria for inclusion were preoperative radiographic template matching with implant size and stem diameter. Exclusion criteria were mental incompetence, significant neurologic, cardiovascular, pulmonary, renal or any other uncontrolled systemic disease, musculoskeletal deformity, any conditions that may prevent or inhibit the patient from performing the activities necessary for data collection, and the presence of any other medical telemetry device. Three subjects were finally selected based on these inclusion and exclusion criteria. Informed consent was obtained from all

patients in accordance with the requirements of the Institutional review board. The demographic data of the three subjects is given in Table 1.

Table 1: Demographic data (of the three subjects implanted with the instrumented device)

Subject	Gender	Age	Weight (Kg)	Height (m)	Surgical Indication
PS	Male	83 y	74	1.80	Primary Osteoarthritis
DM	Male	80 y	80	1.73	Primary Osteoarthritis
SC	Female	65 y	89	1.63	Primary Osteoarthritis

Preoperative preparation: CT scans of the affected lower extremities were obtained preoperatively. These were segmented into 3-dimensional surface models of the femur and tibia in a commercially available software package (MIMICS, Materialise, Belgium). CAD models of various sizes of the knee arthroplasty prosthesis including the custom instrumented tibial prosthesis were obtained from the manufacturer (Zimmer, Warsaw, IN). These models were imported into MIMICS and the size of the implants matching the individual patient was confirmed before surgery. Custom instrumentation (custom reamer, alignment guide, and tibial cutting block) for implanting the instrumented device was developed and tested on cadaver specimens. The selected instrumented implant of appropriate size and side along with the external power induction coil was sterilized using a low-temperature hydrogen peroxide gas plasma-based commercial process (Sterrads, J&J, Raynham, MA).

Intraoperative testing: The tibial bone cut was made at 90° to the long axis in the coronal plane (0° varus) and at 90° in the sagital plane (0° posterior slope). The distal femoral cut was made at 6° valgus to the anatomic axis of the femur. The posterior femoral cut was made at 3° external rotation with reference to the posterior surface of the posterior condyles. Intramedullary alignment was used for femoral and tibial bone preparation. The tibia was reamed with the custom reamer and the instrumented device implanted. Trial femoral components and inserts were implanted to confirm implant size and fit. A standard polyethylene insert (NK-II CR Congruent, Zimmer) and a posterior cruciate-retaining femoral component (NK-II CR, Zimmer) were also implanted using a standard anteromedial approach. The patella was resurfaced with a standard dome-shaped all-polyethylene component. All components were cemented. The external power coil was placed around the patient's leg and wrapped with an elastic bandage. To test implant function, tibial forces were recorded while the operating surgeon manually flexed and extended the knee and applied varus and valgus moments at the knee at 0° and 90° flexion angles. All patients underwent routine postoperative rehabilitation as per a standard primary total knee arthroplasty. All three surgeries were uneventful. The custom prostheses fit adequately and were fully functioning when powered on.

2.E Measurement of Tibial Forces During Early Postoperative Phase

On postoperative day 1, tibial forces were recorded during active and passive knee flexion, active and passive straight-leg raising, and during partial weight bearing with a walker. When the patients were able to walk with the help of a walker, tibial forces were recorded during the patient's first few steps. During the first 2 weeks of

the patient's postoperative recovery, tibial forces were monitored during knee exercise, active and passive knee flexion, standing on both legs with and without support, walking, stair-climbing and rising from a chair when possible. The entire data from the early postoperative phase are not reported in this dissertation and are being analyzed in a separate physical therapy and rehabilitation study to identify the issues of safe exercises during patient recovery. Peak force generated during the first 2 weeks of rehabilitation for some of the activities are shown in Figure 5. Isometric quadriceps contraction and active and passive leg raises were done in the supine position.

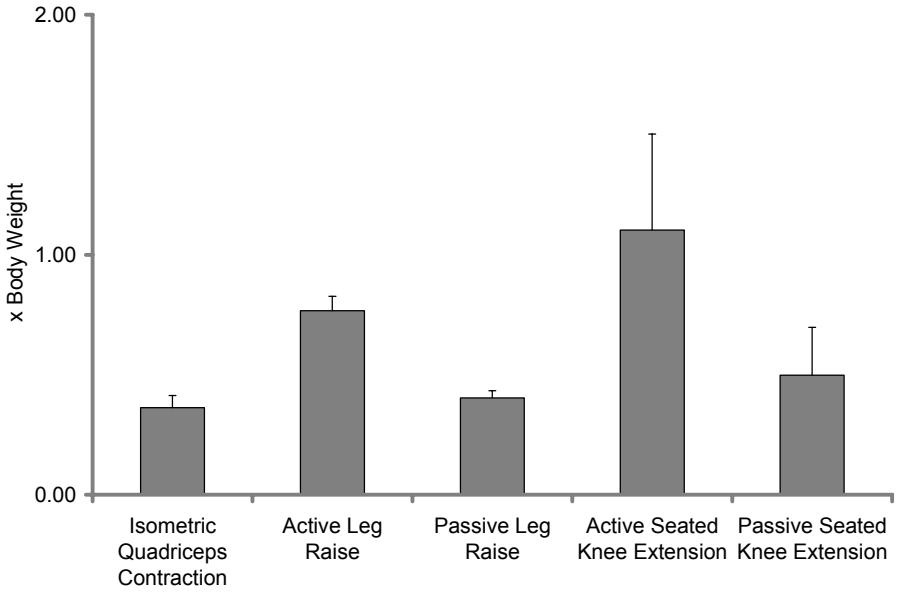

Figure 5A: Peak forces (±SD) generated during the first 2 weeks of rehabilitation for non-weight bearing activities.

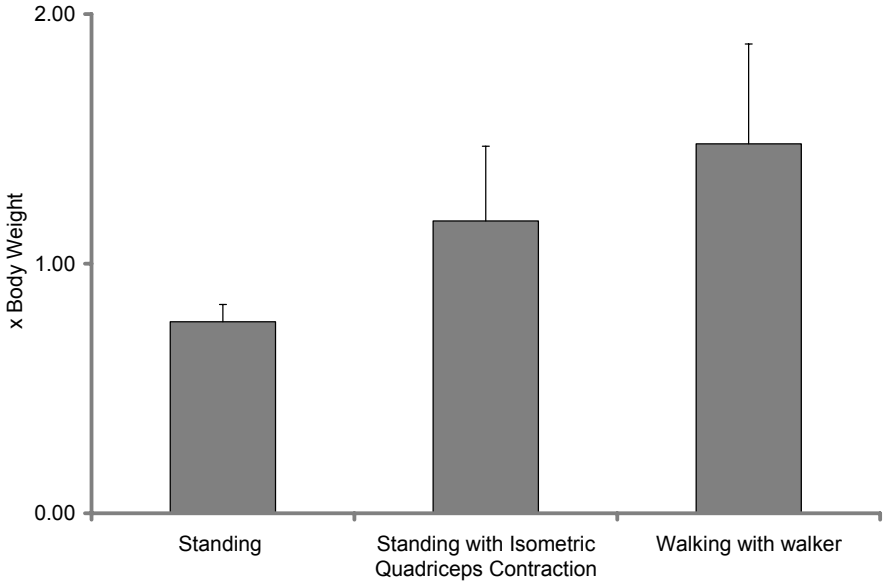

Figure 5B: Peak forces (±SD) generated during the first 2 weeks of rehabilitation for weight bearing activities.

Chapter 3

Tibial Forces During Activities of Daily Living

3.A Abstract

Tibiofemoral loading is very important in cartilage degeneration as well as in component survivorship after total knee arthroplasty. We have previously reported the axial knee forces in vivo. In this study, a second-generation, force-sensing device that measured all six components of tibial forces was implanted in a 74-Kg, 83-year-old male. Video motion analysis, ground reaction forces, and knee forces were measured during walking, stair-climbing, chair-rise, and squat activities. Peak total force was 2.3 times body weight (BW) during walking, 2.5 xBW during chair rise, 3.0 xBW during stair-climbing, and 2.1 xBW during squatting. Peak anterior shear force at the tray was 0.30 xBW during walking, 0.17 xBW during chair rise, 0.26 xBW during stair climbing, and 0.15 xBW during squatting. Peak flexion moment at the tray was 1.9% BWxHt (percentage of body weight multiplied by height) for chair-rise activity and 1.7% BWxHt for squat activity. Peak adduction moment at the tray was –1.1% BWxHt during chair-rise, –1.3% BWxHt during squatting. External knee flexion and adduction moments were substantially greater than flexion and adduction moments at the tray. The axial component of forces predominated especially during the stance phase of walking. Shear forces and moments at the tray were very modest compared to total knee forces. These findings indicate that the soft tissues around the knee absorbed most of the external shear forces. Our results highlight the importance of direct measurements of knee forces.

3.B Introduction

The biomechanics of the knee joint are important in analyzing activities of daily living that primarily involve the lower limbs. The loading of the knee joint correlates with the health of the cartilage, and abnormal loading is associated with development of cartilage degeneration and osteoarthritis (OA). Patient body weight commonly correlates with OA [50]. It has been hypothesized that repeated impulse loading leads to the stiffening of bone with concomitant increased stresses at the cartilage [91]. Subjects with knee OA walk with a greater than normal peak external knee adduction moment [7]. Another hypothesis is that quadriceps fatigue results in reduced shock absorption of knee forces and is the reason for the higher risk of OA in obese women [124]. Regardless of the precise mechanism, it is commonly believed that knee biomechanics play a major role in the etiology of OA.

Total knee arthroplasty is a widely accepted treatment for end-stage arthritis. Knee forces have been shown to affect arthroplasty component survivorship, wear of articular bearing surfaces, and integrity of the bone–implant interface. Excessive knee forces have been implicated in the breakdown of the cement interface or in the collapse of underlying bone. Knee forces along with component design also determine the contact stresses on the bearing surfaces. Contact stresses have been correlated with the magnitude and distribution of wear. Additionally, high-flexion knee designs are being introduced to permit greater knee flexion. These components will allow patients to engage in common activities that involve deep knee flexion such as kneeling, squatting, and sitting cross-legged. Studies analyzing these activities have estimated high knee forces [45,97,129]. Therefore existing knee prosthetic designs may have to be modified to withstand increased loading.

Almost all studies relating to knee forces have involved either in vitro measurements [42,70,121] or estimates using mathematical models [85,94,118,128]. We previously reported the first direct measurement of knee forces in vivo after total knee arthroplasty [32,33]. The tibial component used in that study was instrumented with four load cells that measured the axial components of load on the four quadrants of the tibial tray. This instrumented implant measured the total axial force and the location of the center of pressure. However, shear and moments, which are also important components of knee forces, could not be measured in the first-generation design.

In collaboration with Zimmer, Inc. (Warsaw, IN), we developed a second-generation, force-sensing device that measured all components of tibial forces [74]. The stem of this design was instrumented with strain gages that measured all six components of forces. In this study we report on the first in vivo measurements of shear and moments in the knee after total knee arthroplasty.

3.C Methods

A custom tibial component was manufactured by Zimmer, Inc., based on the Natural Knee II (NK-II) tibial tray design. The tray and locking mechanism were identical to the standard design for implantation with a standard insert. The stem was instrumented with strain gauges to measure three orthogonal forces and three moments. The stem also housed a microtransmitter, which performed analog-to-digital conversion, filtering, and multiplexing before transmitting data via a hermetic glass-feed-through tantalum antenna. External coil induction was used to power the implant. Details of the implant design, strain gages, microtransmitter, telemetry system, and accuracy are give in Chapter 2.

Appropriate institutional review board approval and patient's consent were obtained before implantation in a 74-Kg, 83-year-old male (Fig 6). A standard polyethylene insert (NK-II CR Congruent, Zimmer) and a posterior cruciate-retaining femoral component (NK-II CR, Zimmer) were also implanted using a standard anteromedial approach. The tibial bone cut was made at 90° to the long axis in the coronal plane (0° varus) and at 90° in the sagital plane (0° posterior slope). The distal femoral cut was made at 6° valgus to the anatomic axis of the femur. The posterior femoral cut was made at 3° external rotation with reference to the posterior surface of the posterior condyles. Intramedullary alignment was used for femoral and tibial bone preparation. The patella was resurfaced with a standard dome-shaped all-polyethylene component. All components were cemented. The patient underwent routine postoperative rehabilitation as per a standard primary total knee arthroplasty.

Three months after surgery, knee kinematics, ground reaction forces, and tibial forces and moments were measured in a motion analysis laboratory (Center for

Human Performance, Children's Hospital, San Diego, CA). Knee kinematics were monitored using 6 Vicon cameras and infrared reflective skin markers (Helen Hayes lower limb marker set) [67,68]. Ground reaction forces were measured using 3 force plates (AMTI, Watertown, MA) mounted in the floor of the walkway. Knee kinematics and moments were computed using commercially available software (OrthoTrak, Motion Analysis Corp, Santa Rosa, CA). Data were collected synchronously for the following activities. Walking was studied at a comfortable self-selected pace. Rising from a chair (sit-to-stand) and sitting down in a chair (stand-to-sit) activities were performed with the arms folded across the chest using a chair with a seat height of 44 cm (equal to the joint to floor distance of the patient's knee). Stair-climbing was conducted on stairs with a 17.8 cm (7 in) riser and with hand-rail support. Squatting was performed with both feet parallel to each other, up to a knee flexion angle that was within the patient's tolerance (~ 80°).

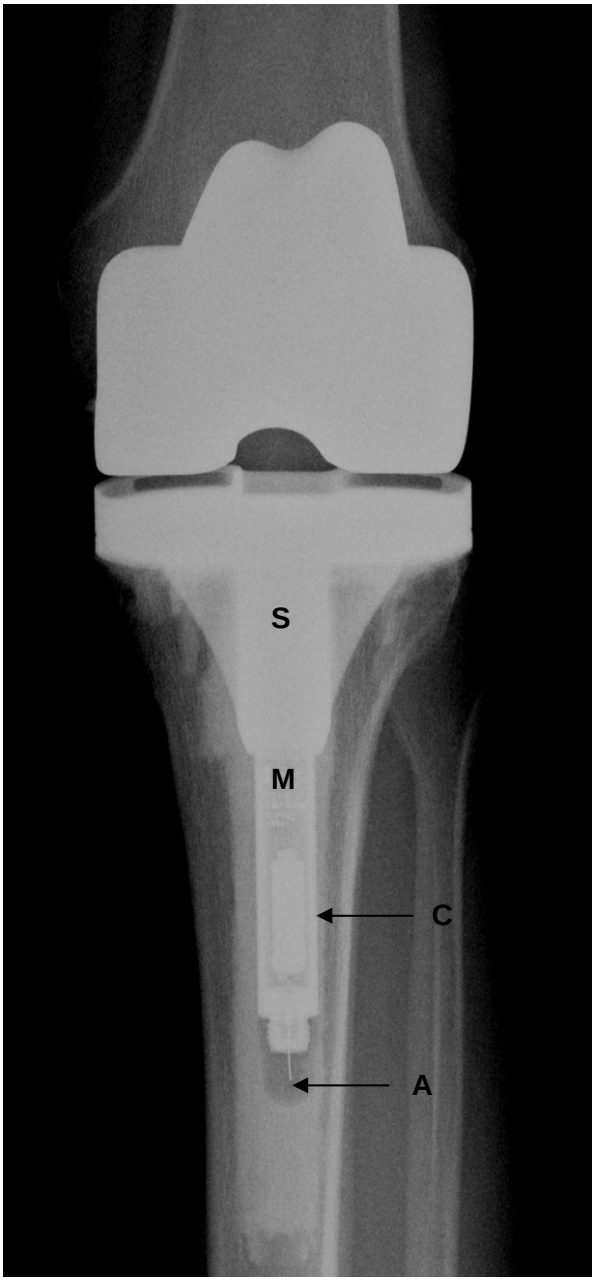

Figure 6: Postoperative radiograph showing the instrumented tibial prosthesis. S: hollow strain-gaged portion of the stem, M: location of microprocessor; C: internal coil; A: transmitting antenna.

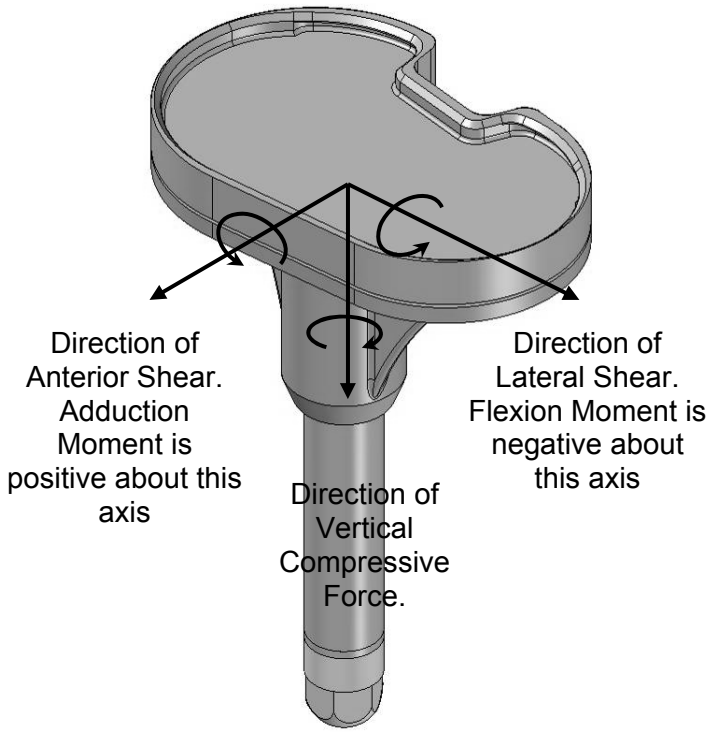

Figure 7: The center of the right hand orthogonal coordinate system was located at the level of the top surface of the tray in line with the center of the cylindrical stem of the prosthesis. The forces and moments acting on the tray were recorded in the directions shown here.

3. D Results

Forces are reported as multiples of body weight (xBW) and moments as a percentage of body weight multiplied by height (% BWxHt). The direction of forces and moments were computed in the coordinate system of the tibial tray (Fig 7), which was implanted at 90° to the intramedullary axis of the tibia in the coronal and the sagital planes. For example, the shear generated at the tibial tray by the femoral component moving in the anterior direction was denoted as anterior shear. Similarly, the moment generated at the tibial tray by adduction of the knee was termed as adduction moment. The peak total tibial forces were between 2 and 3 xBW for the activities studied (Fig 8).

The vertical component of force predominated in all activities (Figs 9–12). For example, during walking, the magnitude of the axial component was on average 86% of the magnitude of the total force. During the stance phase of walking, the vertical component averaged 98% of the magnitude of the total force. Peak anteroposterior (AP) and mediolateral (ML) shear forces were substantially lower than the axial component for all the activities studied. Peak anterior shear force was 0.30 xBW during walking, 0.17 xBW during chair rise, 0.26 xBW during stair-climbing, and 0.15 xBW during squatting. Overall AP shear was mainly directed anteriorly for all activities. During walking and stair-climbing, ML shear was medially directed during the swing phase and during heel strike, changing to a lateral direction early in the stance phase (Figs 9, 10).

External knee moments were measured using ground reaction forces and inverse dynamics. Moments generated at the tibial tray were measured directly by the instrumented tibial prosthesis (Fig 13). External knee flexion moments increased

with knee flexion angle and peaked at 5.7% BWxHt (flexion = 90°) during chair rise and 4.3% BWxHt (flexion = 82°) during squatting. The ground reaction forces under the instrumented side averaged 44 ± 6% of total ground reaction forces for the chair-rise activity and 24 ± 3% for the squat activity. The moment generated by the joint reaction force on the tibial tray peaked at a much lower levels: 1.9% BWxHt for chair-rise activity and 1.7% BWxHt for squat activity. However, a strong linear correlation was noted between the external knee flexion moment and the flexion moment measured at the tibial tray (r^2 = 0.81 for the chair-rise activity, and r^2 = 0.87 for the squat activity).

Peak external knee adduction moments were 3.4% BWxHt for chair-rise activity and 1.8% BWxHt for squat activity. External adduction moments were higher at low flexion angles and decreased with increased knee flexion (Fig 13). Adduction moments measured at the tibial tray were negative and peaked at –1.1% BWxHt during chair rise and –1.3% BWxHt during squatting. The external knee adduction moments correlated poorly with the net moment generated by the joint reaction force at the tibial tray (r^2 = 0.05 for chair-rise activity and r^2 = 0.11 for squat activity).

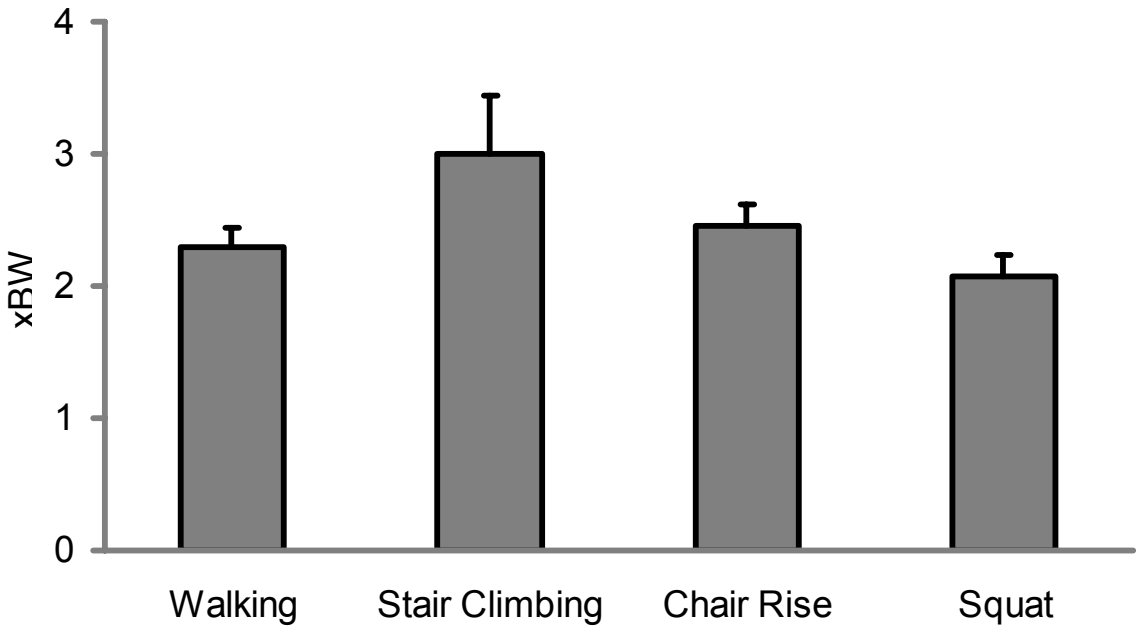

Figure 8: Peak total tibial forces (mean of six cycles for each activity) measured during activities of daily living (error bars represent standard deviations).

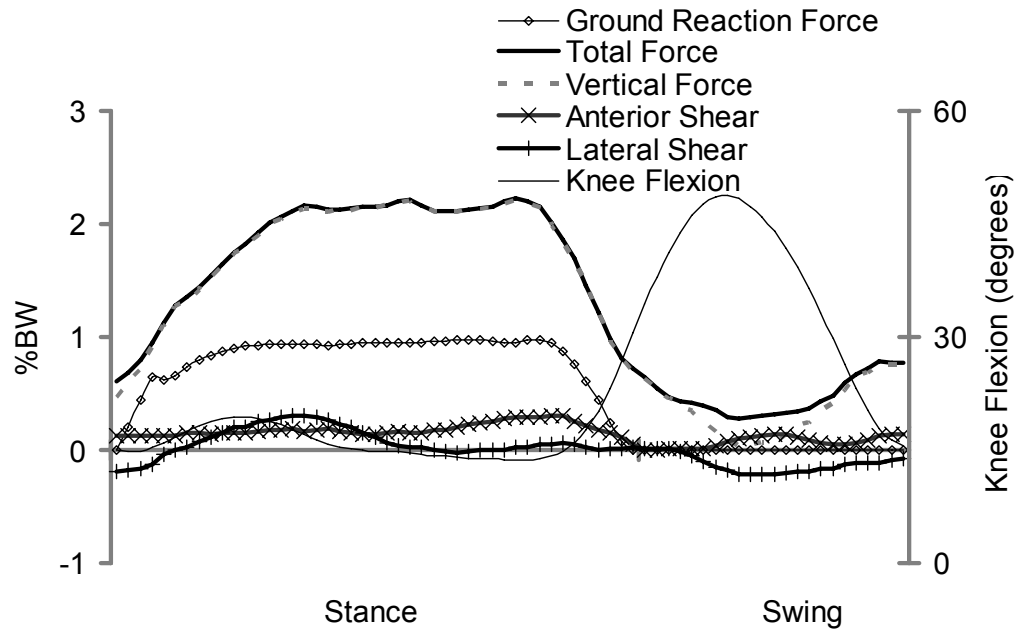

Figure 9: Knee kinematics and forces during one representative walking cycle are shown. The ground reaction force was used to divide the walking cycle into stance and swing phases. The total force was almost entirely comprised of the vertical component of force, especially during the stance phase. Peak anterior shear forces were small (0.3 xBW). Mediolateral shear forces were also in the same range and were laterally directed during most of the stance phase and medially directed during most of the swing phase.

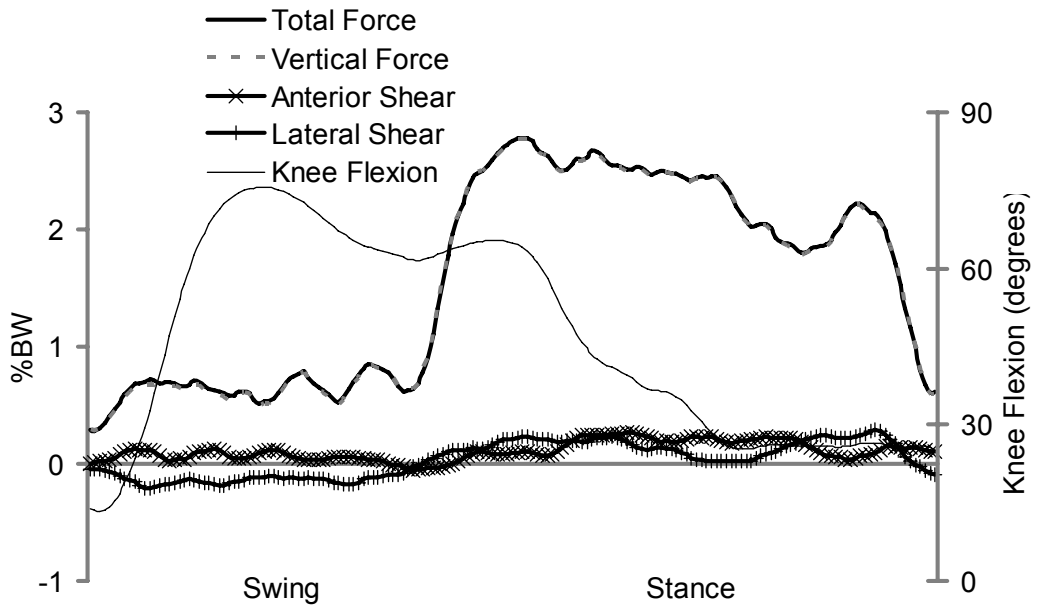

Figure 10: Knee kinematics and forces measured during one representative stair-climbing cycle are shown. As for walking, the total force was almost entirely comprised of the vertical component (the respective plots could not be visually differentiated). Peak anteroposterior shear forces were small (0.26 xBW) and were mainly directed anteriorly. Mediolateral shear forces were laterally directed during most of the stance phase and medially directed during most of the swing phase.

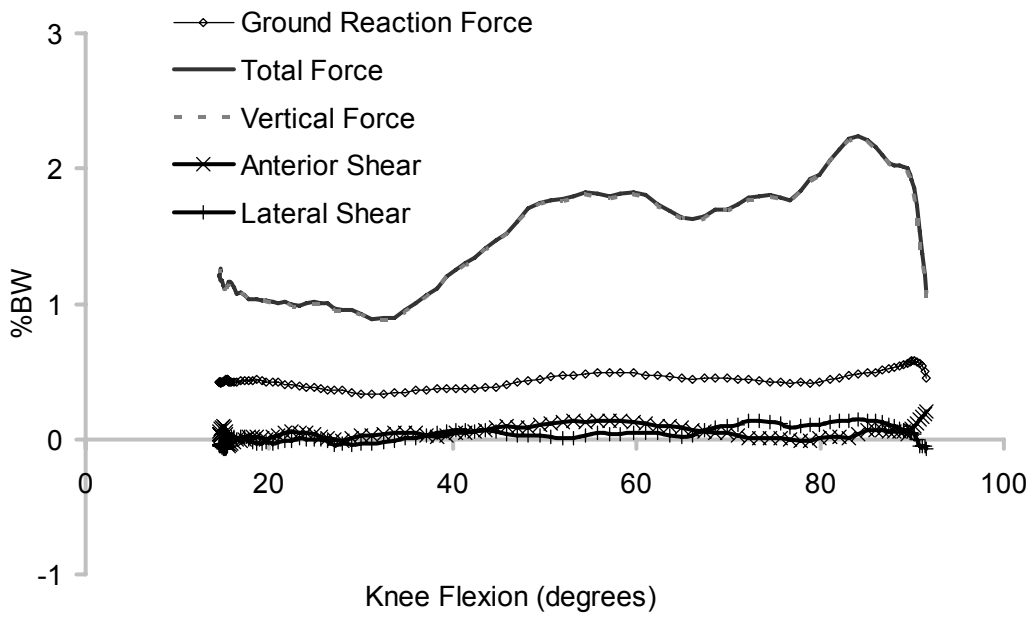

Figure 11: Knee kinematics and forces were measured during one representative chair-rise cycle. Forces are plotted against knee flexion angle. Total force and vertical force components could not be visually differentiated. Peak shear forces were even smaller than for walking and stair-climbing (0.17 xBW). Ground reaction forces under the instrumented limb averaged 44 ± 6% of total ground reaction forces.

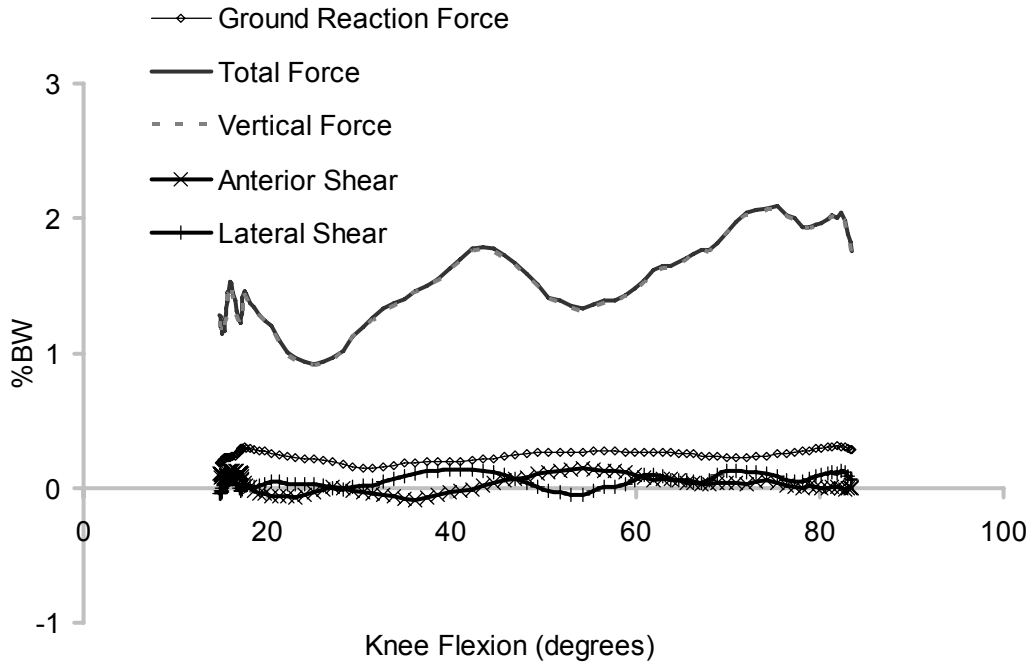

Figure 12: Knee kinematics and forces were measured during one representative squatting cycle. Forces are plotted against knee flexion angle. Peak shear forces were even smaller than for walking and stair-climbing (0.17 xBW). Ground reaction forces under the instrumented side were lower than for the chair activity (24 ± 3% of total ground reaction forces for squat-up and 21 ± 11% for squat-down activities), indicating that the patient was favoring the instrumented knee.

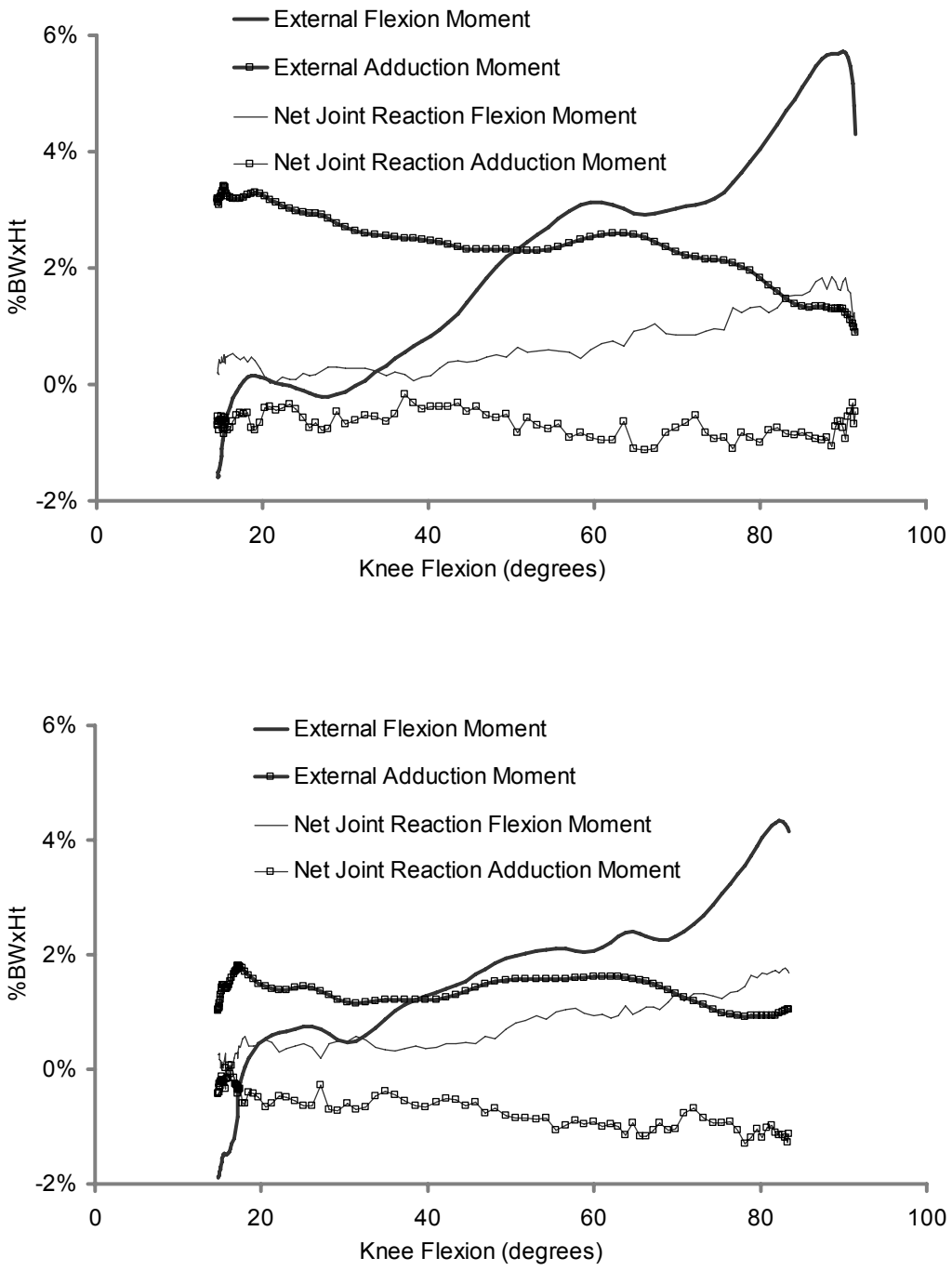

Figure 13: External knee moments (computed from ground reaction forces and knee kinematic data) were typically high. Moments generated by the joint reaction force at the tibial tray were substantially lower. **Top:** Chair-rise activity. **Bottom:** Squat activity.

3E. Discussion

Previously we measured axial knee forces in vivo after total knee arthroplasty [32,33]. However, shear forces and moments are also significant components that affect knee wear and prosthesis survivorship. We therefore developed a second-generation telemetry-enabled tibial prosthesis capable of measuring all six components of force. This is a report of shear and moments measured at the knee joint 3 months after total knee arthroplasty during common activities.

The axial component of forces measured at 3 months peaked between 2 and 3 xBW, which were similar to those measured with the first-generation instrumented tibial prosthesis [32]. The axial component of forces predominated, especially during the stance phase of the activities studied. Shear forces during walking were modest (0.3 xBW) compared to total knee forces. The soft tissues around the knee provide most of the resistance to shear and the intact posterior cruciate ligament may explain the low anterior shear recorded at the tibia tray. Low anteroposterior shear forces during walking (0.40–0.54 xBW) have also been reported at the tibia in a patient with an instrumented distal femoral replacement and a hinged knee design [127]. Another study on the lower limb model in patients with instrumented hip arthroplasties reported peak contact shear forces that averaged 0.5 xBW across four patients [128]. The knees in those patients were not implanted. These shear forces are in the same range as those reported for younger subjects with normal knees, i.e., peak external shear forces (computed with inverse dynamics) averaged 0.39 xBW [97] and 0.33 xBW [27], while peak joint contact shear forces averaged 0.5 xBW [27]. However, knee joint contact forces as high as 2 xBW have also been predicted by mathematical models

[118]. Shear forces measured in the mediolateral direction were also low, which were similar to earlier estimates [94].

Peak tibial forces were substantially higher while climbing stairs (averaging 3 xBW) than for the chair-rise and squat activities. This was possibly because the latter two activities involved a double-legged stance throughout the cycle. For the squat activity, the patient appeared to be loading the instrumented limb less than the contralateral side (as evidenced by the distribution of the ground reaction forces under each foot).

Shear forces were also low for the chair-rise and squat activities despite the higher flexion angles achieved (greater than 80° while squatting and greater than 90° during chair rise). Higher peak external anteroposterior shear forces have been computed in young, normal subjects averaging 0.47 xBW for stair climbing and 0.58-0.63 xBW for squatting [97]. Even higher peak joint contact shear forces (1.2 xBW) have also been reported during stair climbing [27]. Our measurement of low shear forces during these activities again emphasizes the contribution of muscles and ligaments in resisting tibial shear.

We measured moments at the tibial tray for two activities that typically generate high external moments at the knee: rising from a chair and squatting. In young, normal subjects, knee moments were significantly affected by the height of the chair [111]. When compared to normal subjects, OA and knee arthroplasty patients reduced flexion moments by displacing the center of mass anteriorly [123]. This compensation was more pronounced at lower chair heights. At chair seat heights equal to or greater than 100% of the knee joint to floor height, the differences in kinetics of the sit-to-stand activity between normal and total knee arthroplasty patients

cease to exist. We therefore chose a seat height equal to the knee joint-to-floor height. The patient was able to rise from the chair without arm support and demonstrated no significant difficulty. Elderly subjects with chair-rise difficulties typically require a seat height of 120% of the knee joint-to-floor height [135]. Patients with unilateral total knee arthroplasty also tend to shift the center of mass to the normal limb as an additional compensatory maneuver [123]. In the present study, the ground reaction forces under the instrumented side averaged 44 ± 6% of total ground reaction forces, indicating that the center of mass was not substantially shifted to the contralateral side.

Peak external knee flexion moment while rising from a chair was moderately high (5.7% BWxHt). This value was higher than the moments generated by normal, osteoarthritic, or total knee arthroplasty subjects of similar age range [3–4% BWxHt [123]]. The peak external knee moment calculated during the squat activity (4.3% BWxHt) was similar to that reported for healthy subjects in the same age range [4.5% BWxHt [51]]. However, substantially larger peak flexion moments (13.5% BWxHt) have been reported for younger, normal subjects [97]. This is likely due to the difference in peak flexion angle achieved during the squat activity: 150° for young subjects vs. 100° for older subjects. Peak flexion moment measured at the tibial tray was substantially lower (less than 2% BWxHt for both activities).

The peak external adduction moment during chair-rise activity (3.4% BWxHt) was higher than that for squat activity (1.8% BWxHt). Low peak external adduction moments have been reported during chair-rise for older normal subjects (1.15% BWxHt) and for subjects with chronic knee pain [1.31% BWxHt [3]]. Adduction moments at the tibial tray were also low (around 1% BWxHt) and, unlike flexion

moments, correlated poorly with external adduction moments ($r^2 \leq 0.11$ for both activities).

This is a report of knee forces and moments measured in only one patient. Due to patient-to-patient variation and implant design differences, these absolute values cannot be extrapolated to all knee arthroplasty patients. In addition, forces were measured at the 3-month postoperative time-point. We have shown that tibial forces can increase up to 2-years postoperative [32]. Finally, only activities of daily living are reported under carefully controlled laboratory conditions. Forces during other activities and during unanticipated events such as stumbling may be substantially higher than those reported here. We are in the process of implanting more patients with this second-generation implant. We are actively following all patients to increase the duration of follow up, as well as the range of activities analyzed.

Overall, shear forces, as well as moments at the tibial tray, were fairly low. These results indicate that accurate computation of knee contact forces requires appropriate modeling of the passive and active soft tissues. Direct measurements of knee joint reaction forces and moments coupled with robust mathematical models are extremely valuable in increasing our understanding of the loading of the soft tissues, cartilage, and bone of the natural knee, as well as the prosthetic components of the implanted knee.

3.F Acknowledgements

This work was funded in part by NIH grant #5 R21 EB004581-02.

The contents of Chapter 3 have been published in the Journal of Biomechanics: D. D'Lima, S. Patil, N. Steklov, S. Chien, C. Colwell Jr. In vivo knee

moments and shear after total knee arthroplasty. Journal of Biomechanics, Volume 40, Pages S11-S17, 2007

Chapter 4

Development and Validation of a Finite Element Model of Knee Contact

4.A Introduction

Polyethylene is still the most popular bearing material in use for total knee arthroplasty. Despite its widespread use, wear and damage continue to be the major factor implicated in revisions.[120] The yield strength of polyethylene has been reported to range from 13 to 32 MPa,[11,18,25] with even lower values reported for the fatigue strength.[134] Polyethylene wear is also thought to correlate with contact stresses. [89,114]

Contact stresses can often exceed the yield strength of ultra high molecular weight polyethylene.[10,62,80,125] The reported average contact area of a natural knee joint ranges from 765 to 1150 mm^2 which drops to between 80 and 300 mm^2 after total knee arthroplasty depending on the load and design.[53,71,106,108] Reports of peak polyethylene contact stresses have been as high as 30 to 60 MPa: exceeding the yield point for polyethylene.[80,125] These studies on polyethylene contact stresses have been either computed using mathematical models or have been measured in vitro with pressure sensors under estimated knee forces. In vivo measured tibiofemoral force values would therefore be extremely useful in validating these reports.

For the finite element modeling portion of the study we used data from the first patient implanted with the first-generation device. This patient had the longest follow up and data for the most number of activities including fluoroscopic kinematics, ground reaction force measurement, and video motion analysis. Data analysis of the three subjects implanted with the second-generation device indicated that axial loads

comprised more than 95% of the loads during the stance phase of all the activities measured. This validated the data collected from the first generation device which only measured axial loads.

4.B Implant Geometry and Mesh Verification

A finite element model of the knee was constructed using a commercial finite element analysis program (Fig 14, MSC.MARC, MSC.Software, Santa Ana, CA). The femoral component and tibial tray were modeled as rigid bodies. The insert was meshed with hexahedral and pentahedral elements. Optimum mesh density was computed in two stages. Predicted peak contact stresses and contact area in a simplified model of a spherical rigid body indenter with a radius of 14 mm contacting a flat “insert” with a linear elastic modulus of 1000 MPa was compared with an analytic Hertzian contact solution (Fig 15). Convergence of contact area measurement and peak contact stresses within 3% of the analytical solution was achieved with a mesh density using elements with a mean edge length of 0.25 mm. Next, convergence of peak contact stresses for the FEA model using prosthetic component geometry was also obtained with a mean edge length of 0.25 mm.

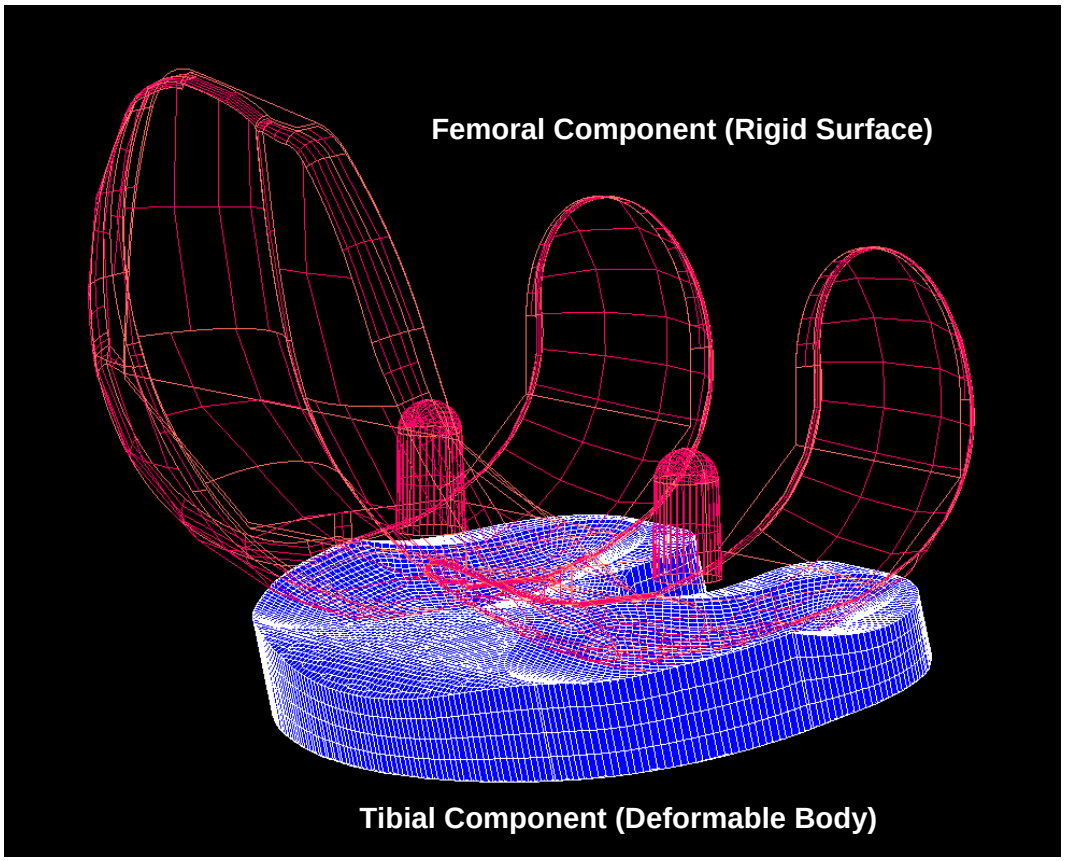

Figure 14: The surface geometry of the prosthetic components was reconstructed by importing CAD models into a commercial finite element program (MSC.MARC). The femoral component and tibial tray were modeled as a rigid surfaces, the tibial insert was modeled as a deformable body with elastoplastic properties to represent polyethylene.

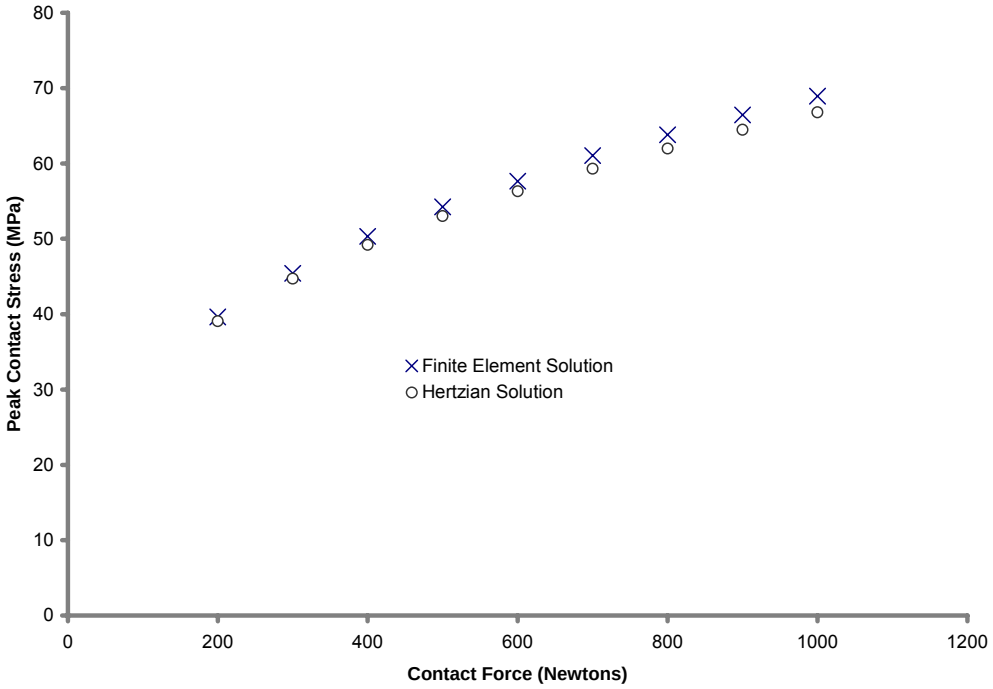

Figure 15: Convergence of contact area measurement and peak contact stresses within 3% of the analytical Hertzian solution was achieved with a mesh density using elements with a mean edge length of 0.25 mm. Shown here are analytic calculations and finite element predictions of peak stresses for a spherical rigid body indenter with a radius of 14 mm loaded against a flat “insert” with a linear elastic modulus of 1000 MPa

4.C UHMWPE Material Properties

Several computational models of artificial joints involving polyethylene as a bearing surface have used linear material models.[10,52,116] However, polyethylene is a complex material exhibiting the plastic flow behavior of a semi-crystalline polymer.[9,55]. The fatigue and fracture potential of polyethylene In tibial components has been related to the yield stress.[79] Under clinically relevant loading conditions polyethylene undergoes large deformations often approaching the theoretical yield limits.

Some models that include plastic behavior have treated polyethylene as an elastic-perfectly plastic material. However, true stress-strain behavior reveals strain hardening, which has been attributed to crystalline transformation.[54] Von Mises stresses are often used to set yield criteria. Below the von Mises yield point, the material behaves in a purely elastic manner. Beyond the yield point, the material exhibits strain-hardening behavior. True stress-strain behavior of polyethylene in uniaxial tension and compression including the yield criterion and the ultimate stress and strain have been previously reported. Based on these considerations, polyethylene was modeled as a nonlinear elastoplastic material using von Mises yield criteria.[79]

4.D Validation of Contact Analysis

For validation, the predicted contact measures (peak stresses and contact area) were compared with those experimentally measured (Tekscan, South Boston, MA) on a multiaxial testing machine (Fig 16, Force-5, AMTI, Watertown, MA). The sensors consisted of a plastic laminated, thin-film (nominally ~100μ thick) electronic pressure transducer (sensor) with two 9.2 cm^2 sensing arrays, each with 2288

sensing elements. A femoral component and insert of the same size and design were obtained from the manufacturer (DePuy Johnson & Johnson). The polyethylene insert test specimen was of the same source, sterilization method, and packaging and was identical to that of the implanted insert. The components were mounted on a multiaxial testing machine (Force-5, AMTI, Watertown, MA). The Tekscan sensor was placed between the articulating surfaces of the medial and lateral compartments and contact stresses and contact area measured with the implants aligned at three different flexion angles (0, 30, and 90) and three axial loads (1000, 2000, and 3000 N). The peak contact stresses were compared to those predicted by the finite element model for the same loading conditions and the mean absolute error was 6% (Fig 17).

The comparison with the analytical Hertzian contact solution served to validate the contact algorithm utilized in MSC.MARC as well to identify the optimal mesh density for a simplified geometry resembling the geometry of unicompartmental tibiofemoral contact. The experimental validation supported the choice of elastoplastic material model for the polyethylene.

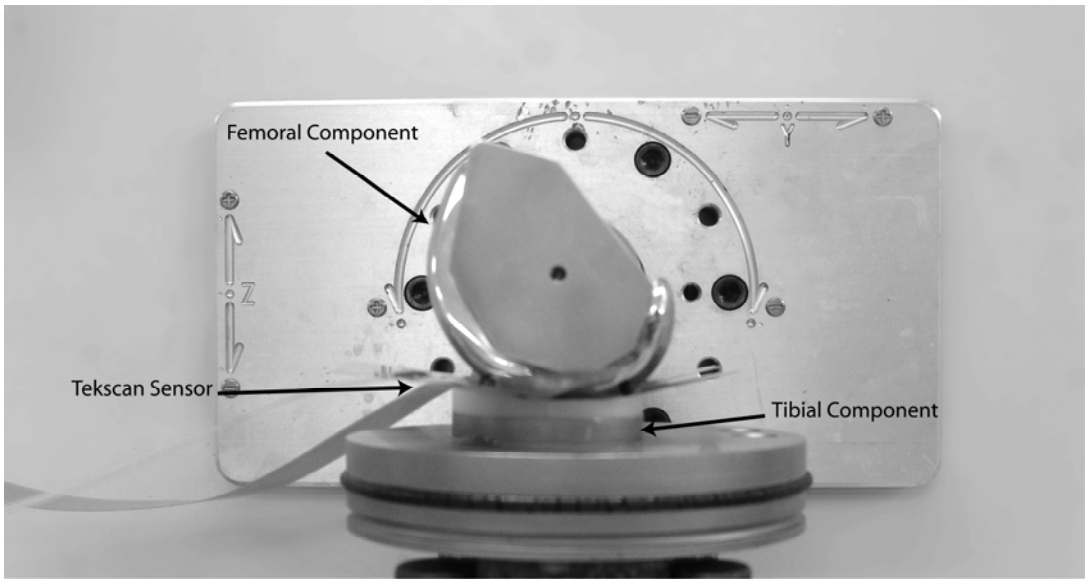

Figure 16: Tekscan pressure sensors were used to validate the finite element model. Knee prosthetic components identical to those implanted in vivo were mounted on a multi-axial testing and loaded under varying degrees of flexion angle and axial force.

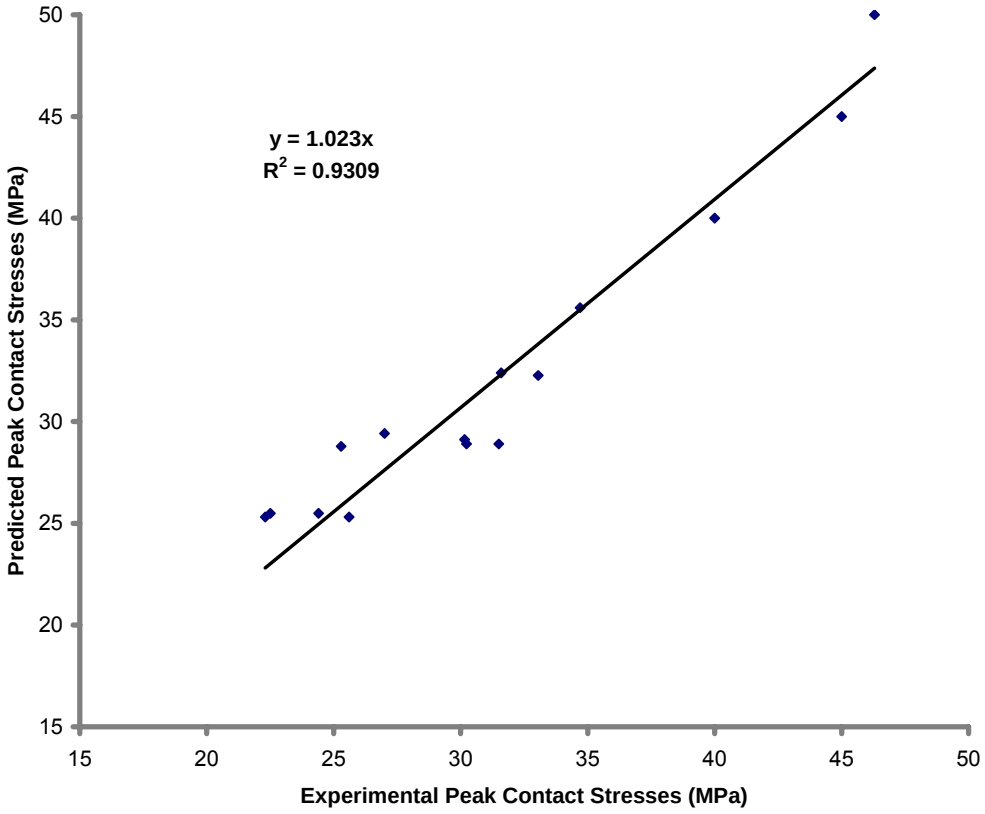

Figure 17: Peak contact stresses measured by the Tekscan sensors were compared against those predicted by the finite element model under the same loading and kinematics conditions. A strong linear correlation (R^2 >0.9), slope = 1.02 validated the selected of the elastoplastic model.

Chapter 5

Contact Stresses Measured During Activities of Daily Living

5.A Data Collection and Processing

The second-generation device validated the axial forces measured by the first-generation device.[31] In addition, more complete data were available and at a later follow up from the patient implanted with the first-generation instrumented device.[30] Therefore we elected to use data from the first generation device for calculation of contact stresses. This patient was 68-Kg, 80-year-old male. An analysis of knee alignment was done on the postoperative standing radiograph. The angle between the bottom surface of the tibial tray and the tibial shaft (i.e., line through the midpoint of the tibial cut and the center of the talus) was 90.1° (the target surgical alignment was 90°) The femoral component was aligned at 6° valgus to the anatomic axis of the femur. The mechanical axis of the lower limb (center of femoral head to center of ankle) passed through a point 5% lateral to the mid-point of the tibial tray. This would indicate that a greater proportion of the total load would pass through the medial compartment of the knee.

Fluoroscopic motion analysis was used to record knee kinematics at the Biomotion Foundation, West Palm Beach, FL. This is a validated method of accurately measured femoral and tibial component position relative to each other.[8,39] Briefly, a shape matching algorithm was used to fit a 3-dimensional surface model of the prosthetic component to its 2-dimensional fluoroscopic image (Fig 18). After fitting the surface models of the femur and tibia, the 3-dimensional position and

orientation relative to each other was recorded. This was done on a frame-by-frame basis yielding dynamic data.

Figure 18A: A shape matching algorithm was used to fit 3D CAD models of the prosthetic components to the 2D silhouette obtained during fluoroscopic imaging. Shown here is the original fluoroscopic image.

Figure 18B: The processed fluoroscopic image has been overlaid with the CAD models oriented at the shaped matched site.

In conjunction with the fluoroscopic motion analysis data, the vertical ground reaction force was also recorded using a force plate mounted on the floor of the laboratory. The three datasets (fluoroscopic kinematics, ground reaction force, and knee force) were compiled and synchronized for the following activities: fast gait, slow gait, stair ascent/descent, kneel, and lunge activities.

Motion cycles were constructed from synchronized data for subsequent data analysis. For the gait activity, the heel strike of the instrumented limb was used to define the limits of the motion cycle. The gait motion cycle was divided into stance phase and swing phase. The stance phase being defined from heel strike to toe-off, and the swing phase being defined from toe-off to the following heel strike. For the stair activity, the motion cycle started when the tibial force began to rise and ended when it returned to its starting value. The mean duration of the resulting motion cycles was 1.11 s for gait and 3.20 s for stair. For the kneel and lunge activities, time frames were analyzed only from the final static pose, which was held by the patient for several seconds and possessed an approximately constant tibial load and knee flexion angle. These two activities were not full weight bearing since the patient was standing on the opposite leg.

For input into the finite element model, one set of kinematic and tibial force data was constructed from the synchronized experimental data for each activity. These representative cycles was created by averaging multiple cycles ($n = 5 – 9$) for each activity. The forces measured at the load cells in each quadrant of the tibial tray were used to calculate the magnitude and the location of the net compressive tibial load. [70] A net resultant axial force acting at the center of pressure for each instant of motion cycle was calculated.

5.B Model Loading and Boundary Conditions

The femoral component was translated and rotated relative to the tibial component using the fluoroscopically derived knee kinematics. A vertical (axial) compressive load was applied at the tibial component. The location and magnitude of this force were obtained from the tibial force data as described in Section 5.A The tibial tray was free to rotate in adduction-abduction and translate in the mediolateral and vertical directions but was fixed in other degrees of freedom. The freedom in adduction-abduction and mediolateral translation was to account for potential error in the fluoroscopic analysis in out-of-plane translations and rotations. [8]

For comparison of contact stresses calculated in vivo with those generated during knee wear testing, we also applied loading and boundary conditions using the ISO-recommended conditions for knee wear simulation.[64] The ISO conditions are representative of normal walking and load the knee up to a maximum of 2600N during the stance phase. Knee flexion reaches a peak of 16° during the stance phase and 58° during the swing phase.

Contact stresses and area were calculated for each of the activities. In addition, the centroids of the medial and lateral contact patches were calculated and the relative femorotibial sliding distance vector was computed for each increment over the entire cycle (100 increments per cycle) of gait, step-up activity, and ISO kinematic waveform. Total relative sliding distances per cycle were averaged across medial and lateral compartments.

5.C Walking

In general, peak and mean contact stresses during gait correlated with the axial load on the tibia. For comparison between conditions the following three events during the gait cycle were chosen: HS = peak tibial load after heel-strike (first peak), TO = peak load before toe-off (second peak), and MS = the lowest load during mid-stance. Peak contact stresses, mean contact stresses, and contact areas for gait at two speeds were similar (Fig 19). The ISO loading waveform applies greater axial load (peak 2600N) and therefore generated higher contact stresses. The peak contact stresses generated during the ISO simulation were associated with the peak before toe-off (30.13 MPa) and were ~18% higher than peak in vivo contact stresses calculated for the fast gait activity. The weight of the subject (68 Kg) was lower than the mean typically reported for total knee arthroplasty patients. Therefore the axial load was scaled up to simulate a subject with a mean body weight of 77 Kg. [112] Peak contacts stresses using a mean body weight of 77 Kg increased by 3.7% and 3.9% for the two peaks compared (just after heel-strike and before toe-off, respectively).

Walking is generally considered an activity that subjects the prosthetic components to benign stresses in a well aligned knee. Our data support this consensus, since peak stresses were below those reported for yield strength of polyethylene. Peak contact stresses for this particular subject were lower than those calculated using the ISO recommended waveform primarily because of the lower axial knee loads (1400 N vs 2600 N ISO-recommended). In this particular subject, peak forces during walking were 2.2 times BW. The subject's body weight (68 Kg) was lower than the mean body weight (~77 kg) reported for primary knee arthroplasty patients in our patient population.[112] However, even when the knee forces were

scaled to represent a more typical knee arthroplasty patient's body weight, the resultant peak contact stresses were lower than those calculated for the ISO-recommended waveform.

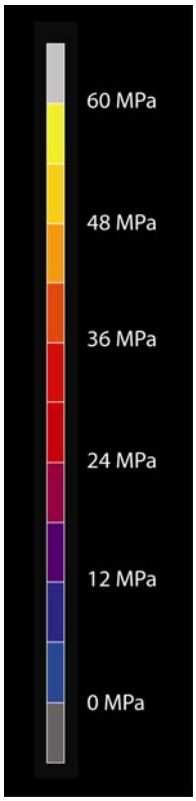

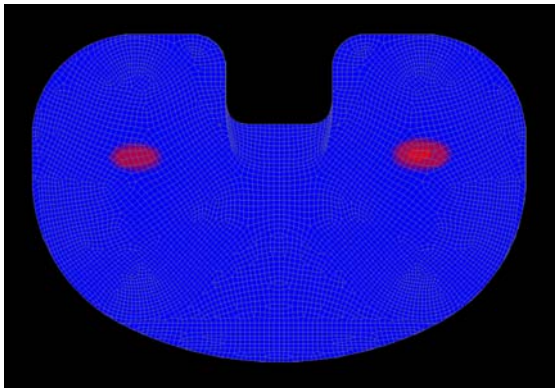

Figure 19A: Contact stresses generated at the first peak of axial force after heel-strike during fast gait.

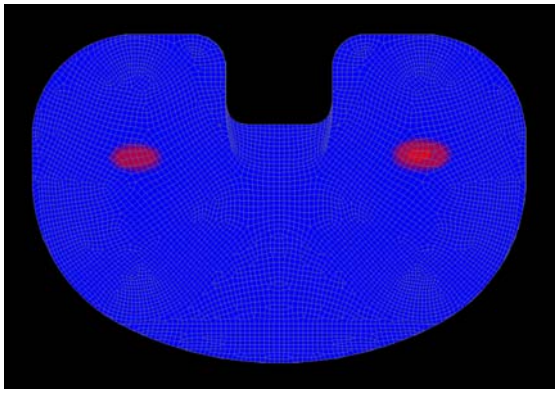

Figure 19B: Contact stresses generated at the first peak of axial force after heel-strike during slow gait.

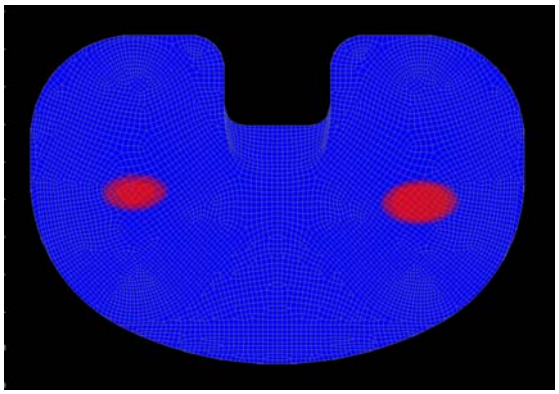

Figure 19C: Contact stresses generated at the first peak of axial force after heel-strike during ISO loading conditions.

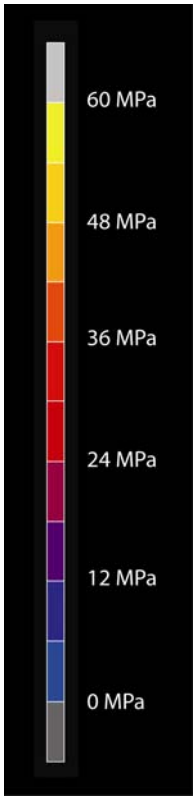

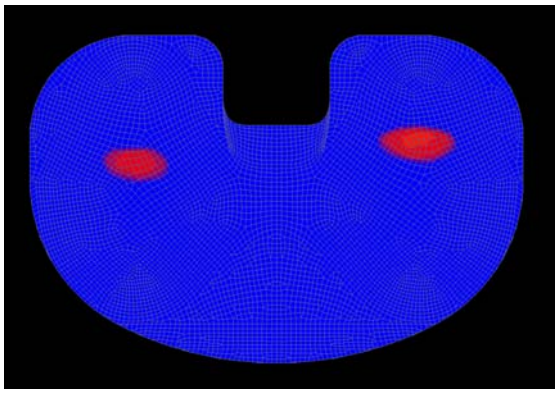

Figure 20A: Contact stresses generated at the peak load during stair-climbing.

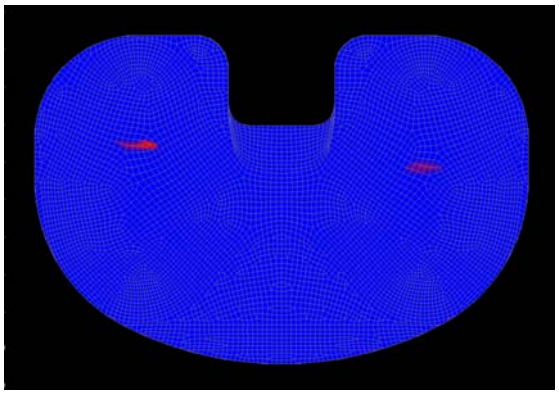

Figure 20B: Contact stresses generated during kneeling.

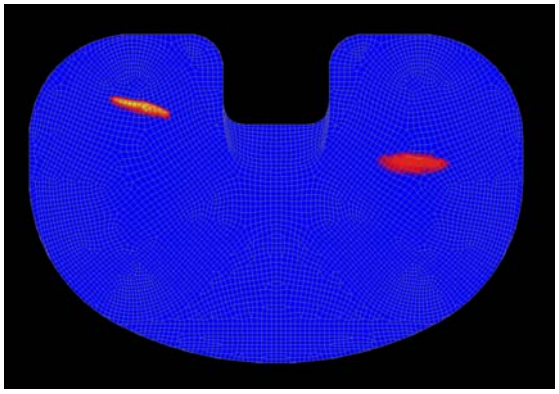

Figure 20C: Contact stresses generated during the lunge activity.

5.D Stair climbing

Stair-climbing is typically associated with higher knee flexion moments than level walking. In this subject, stair-climbing generated higher total contact forces (peak 3.5 xBW). Peak contact stresses were also concomitantly higher (Fig 20). Contact forces peaked with peak knee force as well as peak knee flexion angle. The center of pressure also moved posteriorly with knee flexion indicating the presence of femoral rollback.

Stair-climbing generated higher peak axial forces, which was most likely due to the high external flexion moment since increased axial forces were associated with higher knee flexion angles. However, although peak axial forces during the step-up activity were nearly 60% greater that during gait, peak contact stresses increased by a more modest percentage (18%). This result was most likely due to the inclusion of plasticity in the material model. This resulted in a higher plastic strain during stair-climbing (Fig 23), which contributed to the 29% increase in contact area during stair climbing relative to gait.

5.E Deep Flexion Activities

Two deep flexion activities were studied: kneeling and lunge. The subject had an excellent range of knee flexion by western standards and the fluoroscopically measured flexion angle between the femoral and tibial components was greater than 130° for both these activities. During kneeling most of the external ground reaction force was transmitted through the anterior surface of the upper tibia. In the lunge activity the ground reaction force was transmitted through the foot. The lunge activity generated modest knee contact forces (1.6 xBW) relative to walking and stair-

climbing, however peak contact stresses were the highest recorded for the activities studied (Fig 22). This was due to the reduced contact area in deep flexion (less than 50% of the contact area calculated for stair-climbing). Kneeling generated the lowest contact forces (0.3 xBW) as well as the lowest contact area (29 mm^2) due to the poor femorotibial contact in deep flexion. Despite the low knee forces, kneeling resulted in peak contact stresses that were higher than those calculated for walking or stair-climbing (Fig 22).

The average knee flexion reported for successful total knee arthroplasty is 107 to 120° in western countries [4,19,81,88,110] In eastern and middle-eastern countries, however, a greater degree of knee flexion is desired because deep flexion activities such as squatting, kneeling, and sitting cross-legged are important components of activities of daily living. In western populations also certain activities such as kneeling and gardening are also desirable but cannot always be achieved after total knee arthroplasty because of restricted knee flexion. This has led to several design improvements that are targeted at increasing the range of knee flexion. It has not been conclusively shown that these designs actually increase postoperative range of motion. [73] However, one common design rationale is to modify the articular geometry such that broader contact between the tibial and femoral articular surfaces is maintained at high flexion angles, beyond the 130 to 135° range of generic knee designs. The goal being to distribute the contact stresses in deep flexion. The subject we tested had knee flexion greater than 130° and was able to kneel and perform the lunge activity. As expected, tibial forces were high during the lunge activity and consequently contact stresses were also high. On the other hand, tibial forces were remarkably low during the kneeling activity yet were associated with high

contact stresses because of the small area of contact. This indicates that the so called “high-flexion” knee designs may reduce contact stresses in deep flexion in patients that achieve a high range of postoperative flexion and participate in high flexion activities.

Due to the limited field of fluoroscopic view, only static kneeling poses were possible. However, we also measured tibial forces (without concomitant fluoroscopic motion analysis) during dynamic kneeling (data not shown). A single-limb loading dynamic kneeling activity generated the most tibial forces (as high as 2 times BW). The subject tested did not habitually kneel or sit cross-legged; and therefore, the absolute forces measured may not apply to those patient populations that perform these activities on a daily basis. Nevertheless, the potential for high contact stresses during deep flexion remain significant.

5.F Contact Sliding Distance

The relative femorotibial sliding distance for the entire cycle of walking for this patient was 62 mm, less than that calculated for ISO recommended knee kinematics (83.7 mm). The in vivo sliding distance during the stance phase portion of the cycle was also lower (27.3 mm compared to 38.7 mm for the ISO kinematics). Since wear is a function of contact stresses and sliding distance, the increased sliding distance measured for the ISO kinematic condition indicates that the ISO based wear simulation would generate a higher wear rate than that expected from the kinematic pattern of this subject.

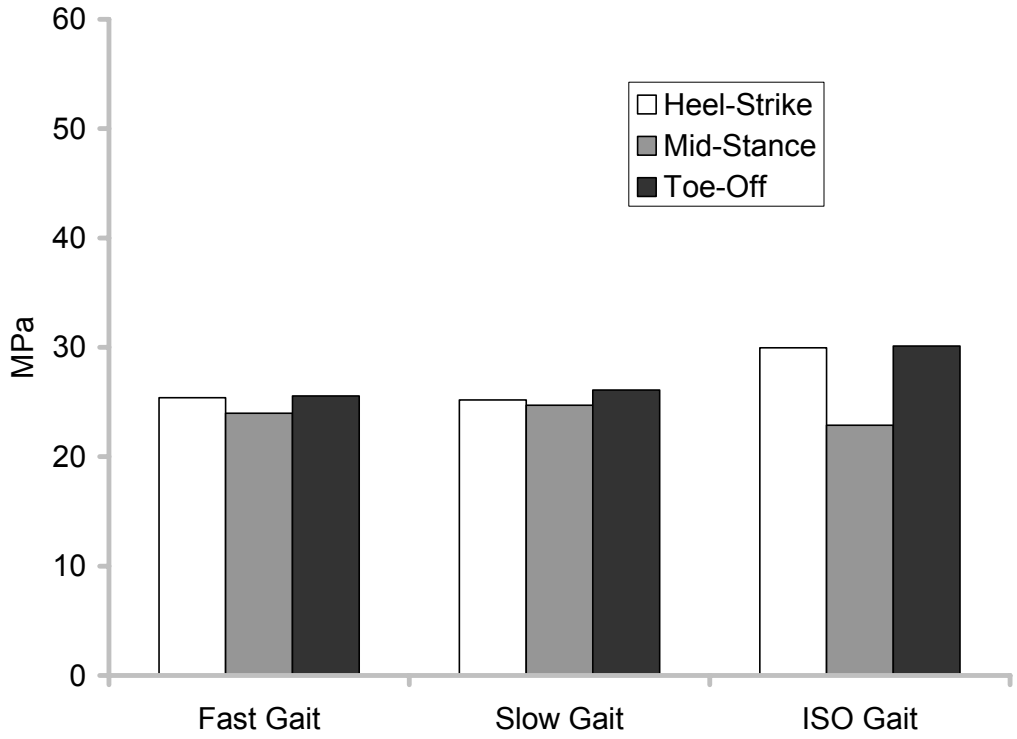

Figure 21: Peak contact stresses were very similar for walking at both speeds. The ISO loading waveform generated ~18% greater contact stresses than walking.

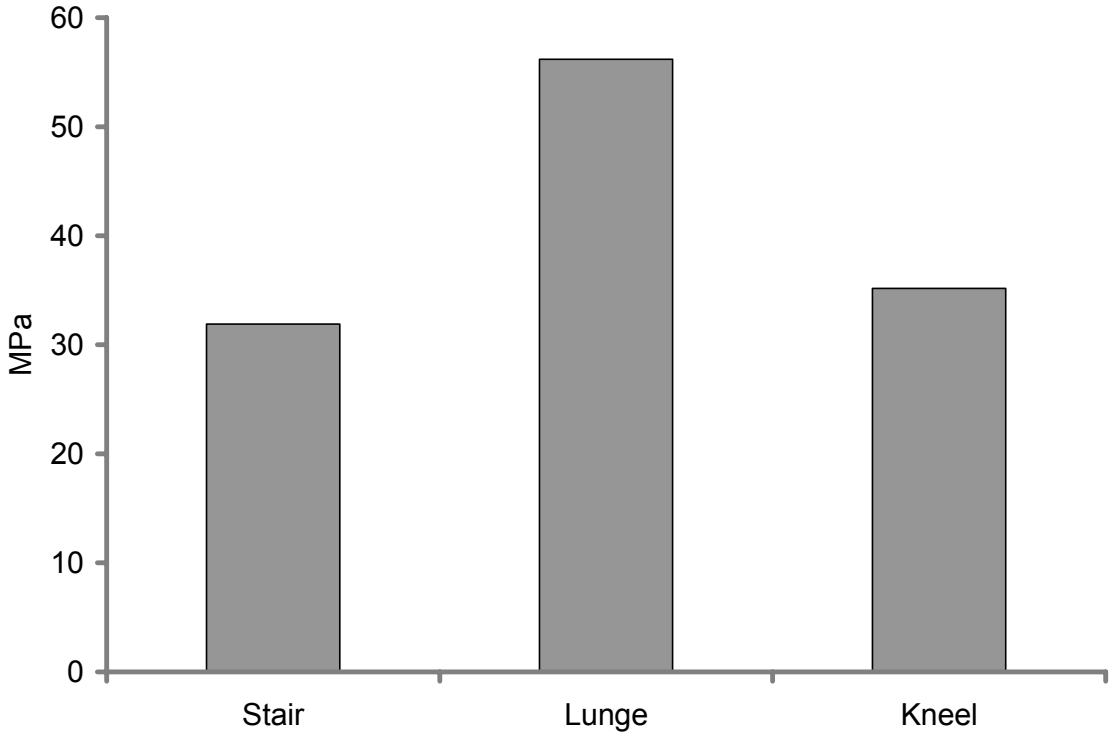

Figure 22: Stair-climbing generated higher contact stresses than walking. However, both high flexion activities (lunge and kneel) generate even higher contact stresses with the lunge activity generating he highest contact stresses.

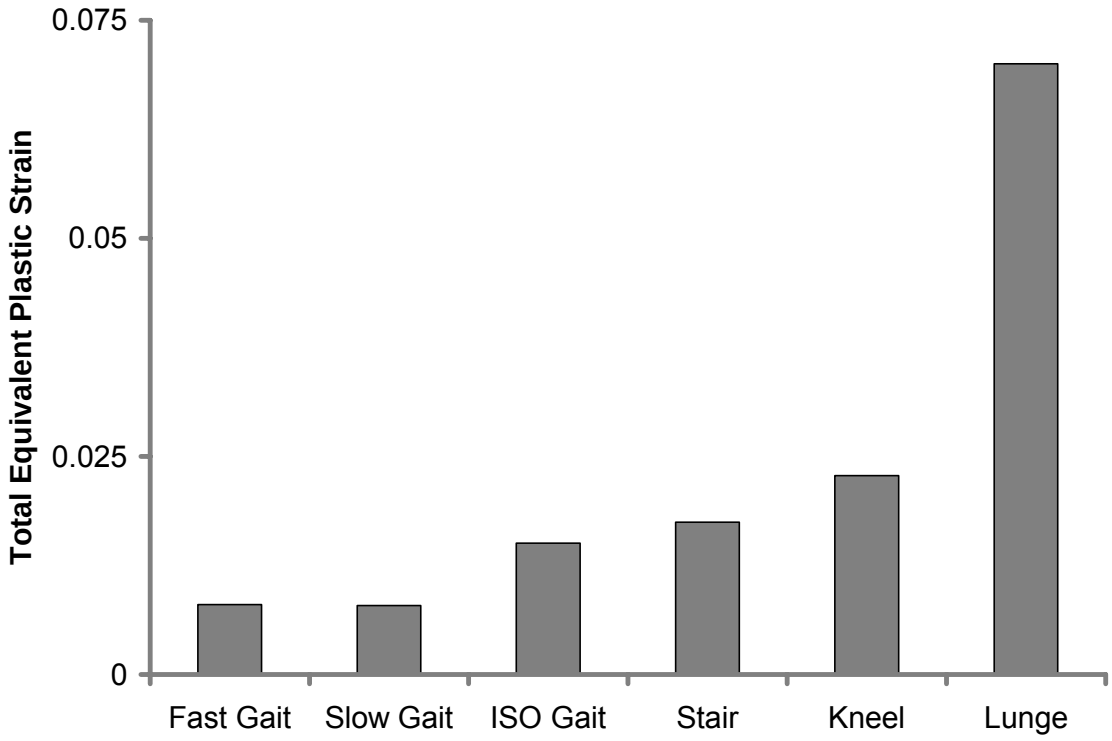

Figure 23: Ranking activities by plastic equivalent strain did not change the order of the activities when compared to ranking based on peak contact stresses. However, the lunge activity was associated by far with the highest plastic equivalent strain.

5.G Damage Stresses

Because the plasticity of the material model was a function of von Mises stresses, these stresses could not be used to assess the potential for polyethylene damage. We therefore calculated the equivalent plastic strain at the insert articular surface and subsurface as a measure of the permanent deformation produced during the activities analyzed. The peak equivalent plastic strain was greater in those conditions associated with higher peak contact stresses. However, the magnitudes did not correlate in a linear fashion: the lunge activity generated peak equivalent plastic strain that was nearly 3 times greater than the other activities (Fig 23).

Peak contact stresses can be used to estimate potential for damage, while average contact stresses are more likely to be associated with potential for wear. Peak contact stresses generated during walking and stair-climbing were similar. The lunge and kneeling conditions generated the highest peak contact stresses and were therefore more likely to be associated with increased risk of polyethylene damage. Plastic deformation under high stresses tends to increase contact area and may partially counteract the substantial increases in contact stresses that would occur in a purely elastic material. Therefore we also used equivalent plastic strain to determine potential for damage. Using plastic strain did not alter the ranking of activities in order of damage potential. However, the lunge activity generated dramatically higher peak equivalent plastic strain than the other activities. Peak plastic strain during kneeling was only slightly higher than that calculated for stair-climbing.

5.H Model Limitations

These results have only been obtained from one patient and the values cannot be generalized to all total knee arthroplasty patients. Knee forces were scaled up to estimate contact stresses if the patient's body weight was similar to the mean body weight reported for total knee arthroplasty patients. However, other individuals may generate forces equaling different multiples of body weight at the knee. [128] Only axial loads were measured in vivo in this subject. However, we have data to indicate that axial loads comprise >95% of the loads generated at the knee for the activities reported in this study. [31] Finally, these data were collected at a single postoperative time period. Ongoing recovery from surgery and increased strength with rehabilitation and exercise may alter the magnitude and distribution of loads. Nevertheless, the changes with time are likely to be small.[32]

Chapter 6

Summary, Clinical Relevance and Conclusions

Tibial forces are directly related to the transmission of stresses in the implant. These include contact stresses generated at the bearing surface and subsurface, stresses at the implant-cement-bone interface and stresses transmitted to underlying bone. Stresses at the bearing surface are a major factor in generating wear and fatigue, which determine the life of the implant. Stresses at the implant-cement interface have been correlated with aseptic loosening, implant migration, and the generation of third-body-wear particles. Stresses transmitted to underlying bone affect remodeling, stress shielding and osteoporosis. By directly measuring these forces, the stresses generated during common activities of daily living can be calculated.

This dissertation is a report of the first measurements of tibial forces, shear, and moments in vivo during activities of daily living, and rehabilitation. The axial component of forces predominated, especially during the stance phase of the activities studied. During walking forces peaked between 2 and 3 xBW. Peak tibial forces were substantially higher while climbing stairs (averaging 3 xBW) than for the chair-rise and squat activities. Overall, shear forces, as well as moments at the tibial tray, were fairly low. The soft tissues around the knee provide most of the resistance to shear and the intact posterior cruciate ligament may explain the low anterior shear recorded at the tibia tray. These results indicate that accurate computation of knee contact forces requires appropriate modeling of the passive and active soft tissues. Direct measurements of knee joint reaction forces and moments coupled with robust

mathematical models can be extremely valuable in increasing our understanding of the loading of the prosthetic components of the implanted knee. This information is invaluable in determining the safety of activities and exercises and can be used to develop more effective rehabilitation programs.

This is the first finite element model of the knee to utilize in vivo data to calculate polyethylene contact stresses in vivo. Walking and stair climbing generated peak contact stresses below the threshold that is generally considered safe for polyethylene. Contact stresses and sliding paths generated in vivo during gait were lower than those generated by ISO-recommended wear simulation indicating that the ISO standards are reasonably representative of a benign activity in a well-aligned knee. Knee kinematics and forces during stair ascent and descent may be also be used to develop more relevant wear simulator protocols. Contact stresses generated during high flexion activities were substantially higher and largely due to the reduced contact area in deep flexion rather than an increase in contact forces. These results support the use of “high-flex” designs that improve contact conditions and preserve contact area at high flexion angles.

These data are also being made available to the orthopaedic scientific community and several collaborations are actively ongoing to validate existing models of the knee that estimate joint forces or to develop more accurate computational models. Once validated, these models can provide valuable information that may lead to design changes that can improve the function and longevity of total knee prostheses. Tibial forces along with the kinematic patterns of the knee have a significant effect on the type and quantity of wear produced.[16,30] In conjunction with simultaneously measured motion data and external forces, in vivo tibiofemoral force

data may also be used to design more effective knee testing rigs and wear simulators that can accurately model knee function and prosthetic wear.

Given the current trends in the increase in older population groups and the increase in the rates of total knee arthroplasty, a significant positive impact on clinical outcomes, longevity, and function is anticipated.

References

1. AAOS Dept of Research and Scientific Affairs. AAOS department of Research and Scientific Affairs. 1994.

2. Aglietti, P., Buzzi, R., De Felice, R., and Giron, F.: The Insall-Burstein total knee replacement in osteoarthritis: A 10-year minimum follow-up. J Arthroplasty. 14:560-565, 1999.

3. Amin, S., Luepongsak, N., McGibbon, C. A., LaValley, M. P., Krebs, D. E., and Felson, D. T.: Knee adduction moment and development of chronic knee pain in elders. Arthritis Rheum. 51:371-376, 2004.

4. Anouchi, Y. S., McShane, M., Kelly, F. J., Elting, J., and Stiehl, J.: Range of motion in total knee replacement. Clin Orthop Relat Res. 331:87-92, 1996.

5. Ansari, S., Newman, J. H., and Ackroyd, C. E.: St. Georg sledge for medial compartment knee replacement. 461 arthroplasties followed for 4 (1-17) years. Acta Orthop Scand. 68:430-434, 1997.

6. ASTM F1800-97. Standard Test Method for Cyclic Fatigue Testing of Metal Tibial Tray Component of Total Knee Joint. 2004.

7. Baliunas, A. J., Hurwitz, D. E., Ryals, A. B., Karrar, A., Case, J. P., Block, J. A., and Andriacchi, T. P.: Increased knee joint loads during walking are present in subjects with knee osteoarthritis. Osteoarthritis Cartilage. 10:573-579, 2002.

8. Banks, S. A. and Hodge, W. A.: Accurate measurement of three-dimensional knee replacement kinematics using single-plane fluoroscopy. IEEE Trans Biomed Eng. 43:638-649, 1996.

9. Bartczak, Z., Cohen, R. E., and Argon, A. S.: Evolution of crystalline texture of high-density polyethylene during uniaxial compression. Macromolecules. 25:4692-4704, 1992.

10. Bartel, D. L., Bicknell, V. L., and Wright, T. M.: The effect of conformity, thickness, and material on stresses in ultra-high molecular weight components for total joint replacement. J Bone Joint Surg Am. 68A:1041-1051, 1986.

11. Bartel, D. L., Rawlinson, J. J., Burstein, A. H., Ranawat, C. S., and Flynn, W. F., Jr.: Stresses in polyethylene components of contemporary total knee replacements. Clin Orthop Relat Res. 317:76-82, 1995.

12. Bassey, E. J., Littlewood, J. J., and Taylor, S. J.: Relations between compressive axial forces in an instrumented massive femoral implant, ground reaction forces, and integrated electromyographs from vastus lateralis during various 'osteogenic' exercises. J Biomech. 30:213-223, 1997.

13. Bergmann, G., Graichen, F., and Rohlmann, A.: Hip joint loading during walking and running, measured in two patients. J Biomech. 26:969-990, 1993.

14. Bergmann, G., Graichen, F., Siraky, J., Jendrzynski, H., and Rohlmann, A.: Multichannel strain gauge telemetry for orthopaedic implants. J Biomech. 21:169-176, 1988.

15. Bloebaum, R. D., Nelson, K., Dorr, L. D., Hofmann, A. A., and Lyman, D. J.: Investigation of early surface delamination observed in retrieved heat-pressed tibial inserts. Clin Orthop Relat Res. 269:120-127, 1991.

16. Blunn, G. W., Walker, P. S., Joshi, A., and Hardinge, K.: The dominance of cyclic sliding in producing wear in total knee replacements. Clin Orthop Relat Res. 273:253-260, 1991.

17. Brand, R. A., Pedersen, D. R., Davy, D. T., Kotzar, G. M., Heiple, K. G., and Goldberg, V. M.: Comparison of hip force calculations and measurements in the same patient. J Arthroplasty. 9:45-51, 1994.

18. Buechel, F. F., Pappas, M. J., and Makris, G.: Evaluation of contact stress in metal-backed patellar replacements. A predictor of survivorship. Clin Orthop Relat Res. 273:190-197, 1991.

19. Buehler, K. O., Venn-Watson, E., D'Lima, D. D., and Colwell, C. W., Jr.: The press-fit condylar total knee system: 8- to 10-year results with a posterior cruciate-retaining design. J Arthroplasty. 15:698-701, 2000.

20. Bugbee, W. D., Ammeen, D. J., Parks, N. L., and Engh, G. A.: 4- to 10-year results with the anatomic modular total knee. Clin Orthop Relat Res.158-165, 1998.

21. Calisse, J., Rohlmann, A., and Bergmann, G.: Estimation of trunk muscle forces using the finite element method and in vivo loads measured by telemeterized internal spinal fixation devices. J Biomech. 32:727-731, 1999.

22. Cameron, H. U. and Hunter, G. A.: Failure in total knee arthroplasty: mechanisms, revisions, and results. Clin Orthop Relat Res.141-146, 1982.

23. Cameron, H. U. and Jung, Y. B.: Noncemented, porous ingrowth knee prosthesis: the 3- to 8-year results. Can J Surg. 36:560-564, 1993.

24. Collier, J. P., Mayor, M. B., McNamara, J. L., Surprenant, V. A., and Jensen, R. E.: Analysis of the failure of 122 polyethylene inserts from uncemented tibial knee components. Clin Orthop Relat Res. 273:232-242, 1991.

25. Collier, J. P., Mayor, M. B., Surprenant, V. A., Surprenant, H. P., Dauphinais, L. A., and Jensen, R. E.: The biomechanical problems of polyethylene as a bearing surface. Clin Orthop Relat Res. 261:107-113, 1990.

26. Collins, J. J.: The redundant nature of locomotor optimization laws. J Biomech. 28:251-267, 1995.

27. Costigan, P. A., DeLuzio, K. J., and Wyss, U. P.: Knee and hip kinetics during normal stair climbing. Gait. Posture. 16:31-37, 2002.

28. Crowninshield, R. D. and Brand, R. A.: A physiologically based criterion of muscle force prediction in locomotion. J Biomech. 14:793-801, 1981.

29. D'Lima, D. D., Chen, P. C., and Colwell, C. W., Jr.: Polyethylene contact stresses, articular congruity and knee alignment. Clin Orthop Relat Res. 392:232-238, 2001.

30. D'Lima, D. D., Hermida, J. C., Chen, P. C., and Colwell, C. W., Jr.: Polyethylene wear and variations in knee kinematics. Clin Orthop Relat Res. 392:124-130, 2001.

31. D'Lima, D. D., Patil, S., Steklov, N., Chien, S., and Colwell, C. W., Jr.: In vivo knee moments and shear after total knee arthroplasty. J Biomech. 2007.

32. D'Lima, D. D., Patil, S., Steklov, N., Slamin, J. E., and Colwell, C. W., Jr.: THE CHITRANJAN RANAWAT AWARD: In Vivo Knee Forces after Total Knee Arthroplasty. Clin Orthop Relat Res. 440:45-49, 2005.

33. D'Lima, D. D., Patil, S., Steklov, N., Slamin, J. E., and Colwell, C. W., Jr.: The HAP Paul Award: Tibial forces measured in vivo after total knee arthroplasty. J Arthroplasty. 21:255-262, 2006.

34. D'Lima, D. D., Patil, S., Steklov, N., Slamin, J. E., and Colwell, C. W., Jr.: Tibial forces measured in vivo after total knee arthroplasty. J Arthroplasty. 21:255-262, 2006.

35. D'Lima, D. D., Slamin, J. E., Morris, B. A., and Colwell, C. W., Jr. An implantable telemetry system to measure intraarticular tibial forces. Trans 45th Orthop Res Soc. 24. 1999.

36. D'Lima, D. D., Townsend, C. P., Arms, C. W., Morris, B. A., and Colwell, C. W., Jr.: An implantable telemetry device to measure intra-articular tibial forces. J Biomech. 38:299-304, 2005.

37. Data Analyst Group. Ingenix. Columbus, OH. 1999.

38. Davy, D. T., Kotzar, G. M., Brown, R. H., Heiple, K. G., Goldberg, V. M., Heiple, K. G., Jr., Berilla, J., and Burstein, A. H.: Telemetric force measurements across the hip after total arthroplasty. J Bone Joint Surg Am. 70A:45-50, 1988.

39. Dennis, D. A., Komistek, R. D., and Mahfouz, M. R.: In vivo fluoroscopic analysis of fixed-bearing total knee replacements. Clin Orthop Relat Res.114-130, 2003.

40. Diduch, D. R., Insall, J. N., Scott, W. N., Scuderi, G. R., and Font-Rodriguez, D.: Total knee replacement in young, active patients. Long-term follow-up and functional outcome. J Bone Joint Surg Am. 79A:575-582, 1997.

41. Diduch, D. R., Scuderi, G. R., Scott, W. N., Insall, J. N., and Kelly, M. A.: The efficacy of arthroscopy following total knee replacement. Arthroscopy. 13:166-171, 1997.

42. Ellis, M. I., Seedhom, B. B., and Wright, V.: Forces in the knee joint whilst rising from a seated position. J Biomed Eng. 6:113-120, 1984.

43. Engh, G. A., Dwyer, K. A., and Hanes, C. K.: Polyethylene wear of metal-backed tibial components in total and unicompartmental knee prostheses. J Bone Joint Surg Br. 74:9-17, 1992.

44. English, T. A. and Kilvington, M.: In vivo records of hip loads using a femoral implant with telemetric output (a preliminary report). J Biomed Eng. 1:111-115, 1979.

45. Escamilla, R. F.: Knee biomechanics of the dynamic squat exercise. Med Sci Sports Exerc. 33:127-141, 2001.

46. Estupinan, J. A., Bartel, D. L., and Wright, T. M.: Residual stresses in ultra-high molecular weight polyethylene loaded cyclically by a rigid moving indenter in nonconforming geometries. J Orthop Res. 16:80-88, 1998.

47. Ezzet, K. A., Hershey, A. L., D'Lima, D. D., Irby, S. E., Kaufman, K. R., and Colwell, C. W., Jr.: Patellar tracking in total knee arthroplasty: inset versus onset design. J Arthroplasty. 16:838-843, 2001.

48. Falatyn, S., Lachiewicz, P. F., and Wilson, F. C.: Survivorship analysis of cemented total condylar knee arthroplasty. Clin Orthop Relat Res. 317:178-184, 1995.

49. Fehring, T. K., Odum, S., Griffin, W. L., Mason, J. B., and Nadaud, M.: Early failures in total knee arthroplasty. Clin Orthop Relat Res.315-318, 2001.

50. Felson, D. T., Zhang, Y., Hannan, M. T., Naimark, A., Weissman, B., Aliabadi, P., and Levy, D.: Risk factors for incident radiographic knee osteoarthritis in the elderly: the Framingham Study. Arthritis Rheum. 40:728-733, 1997.

51. Flanagan, S., Salem, G. J., Wang, M. Y., Sanker, S. E., and Greendale, G. A.: Squatting exercises in older adults: kinematic and kinetic comparisons. Med Sci Sports Exerc. 35:635-643, 2003.

52. Fregly, B. J., Sawyer, W. G., Harman, M. K., and Banks, S. A.: Computational wear prediction of a total knee replacement from in vivo kinematics. J Biomech. 38:305-314, 2005.

53. Fukubayashi, T. and Kurosawa, H.: The contact area and pressure distribution pattern of the knee. A study of normal and osteoarthrotic knee joints. Acta Orthop Scand. 51:871-879, 1980.

54. G'Sell, C. and Jonas, J. J.: Determination of the plastic behaviour of solid polymers at constant true strain rate. Journal of Materials Science. 14:583-591, 1979.

55. G'Sell, C., Paysant-Le Roux, B., Dahoun, A., and et al: Plastic behavior and resistance to wear of ultra-high molecular weight polyethylene. Deformation Yield Fracture of Polym. 10:57-60, 1997.

56. Gere, J. M. and Timoshenko, S. P.: Mechanics of Materials. Ed. 4th Ed. PWS Publishing Company, 1997.

57. Grady-Benson, J., Kaufman, K. R., Irby, S. E., and Colwell, C. W., Jr. The influence of joint line location on tibiofemoral forces after total knee arthroplasty. Trans 38th Orthop Res Soc. 18, 324. 1992.

58. Graichen, F. and Bergmann, G.: Four-channel telemetry system for in vivo measurement of hip joint forces. J Biomed Eng. 13:370-374, 1991.

59. Graichen, F., Bergmann, G., and Rohlmann, A.: Hip endoprosthesis for in vivo measurement of joint force and temperature. J Biomech. 32:1113-1117, 1999.

60. Halloran, J. P., Petrella, A. J., and Rullkoetter, P. J.: Explicit finite element modeling of total knee replacement mechanics. J Biomech. 38:323-331, 2005.

61. Hodge, W. A., Carlson, K. L., Fijan, R. S., Burgess, R. G., Riley, P. O., Harris, W. H., and Mann, R. W.: Contact pressures from an instrumented hip endoprosthesis. J Bone Joint Surg Am. 71A:1378-1386, 1989.

62. Hood, R. W., Wright, T. M., and Burstein, A. H.: Retrieval analysis of total knee prostheses: A method and its application to 48 total condylar prostheses. J Biomed Mater Res. 17:829-842, 1983.

63. Huang, C. H., Young, T. H., Lee, Y. T., Jan, J. S., and Cheng, C. K.: Polyethylene failure in New Jersey low-contact stress total knee arthroplasty. J Biomed Mater Res. 39:153-160, 1998.

64. International Standards Organization. International Standards Organization, standard number 14243-1: Implants for Surgery; Wear of Total Knee Joint Prostheses: Part I: Loading and Displacement Parameters for Wear Testing Machines with Load Control and Corresponding Environmental Conditions for Test. Geneva, Switzerland, International Standards Organization 2000.

65. Jazrawi, L. M., Kummer, F. J., and Dicesare, P. E.: Alternative bearing surfaces for total joint arthroplasty. J Am Acad Orthop Surg. 6:198-203, 1998.

66. Jones, S. M., Pinder, I. M., Moran, C. G., and Malcolm, A. J.: Polyethylene wear in uncemented knee replacements. J Bone Joint Surg Br. 74:18-22, 1992.

67. Kadaba, M. P., Ramakrishnan, H. K., and Wootten, M. E.: Measurement of lower extremity kinematics during level walking. J Orthop Res. 8:383-392, 1990.

68. Kadaba, M. P., Ramakrishnan, H. K., Wootten, M. E., Gainey, J., Gorton, G., and Cochran, G. V.: Repeatability of kinematic, kinetic, and electromyographic data in normal adult gait. J Orthop Res. 7:849-860, 1989.

69. Kaufman, K. R., An, K. N., Litchy, W. J., Morrey, B. F., and Chao, E. Y.: Dynamic joint forces during knee isokinetic exercise. Am J Sports Med. 19:305-316, 1991.

70. Kaufman, K. R., Kovacevic, N., Irby, S. E., and Colwell, C. W., Jr.: Instrumented implant for measuring tibiofemoral forces. J Biomech. 29:667-671, 1996.

71. Kettelkamp, D. B. and Jacobs, A. W.: Tibiofemoral contact area--determination and implications. J Bone Joint Surg Am. 54:349-356, 1972.

72. Kilgus, D. J., Moreland, J. R., Finerman, G. A., Funahashi, T. T., and Tipton, J. S.: Catastrophic wear of tibial polyethylene inserts. Clin Orthop Relat Res. 273:223-231, 1991.

73. Kim, Y. H., Sohn, K. S., and Kim, J. S.: Range of motion of standard and high-flexion posterior stabilized total knee prostheses. A prospective, randomized study. J Bone Joint Surg Am. 87:1470-1475, 2005.

74. Kirking, B., Krevolin, J., Townsend, C., Colwell C.W., J., and D'Lima, D. D.: A multiaxial force-sensing implantable tibial prosthesis. J Biomech. 39:1744-1751, 2006.

75. Knight, J. L., Atwater, R. D., and Guo, J.: Early failure of the porous coated anatomic cemented unicompartmental knee arthroplasty. Aids to diagnosis and revision. J Arthroplasty. 12:11-20, 1997.

76. Kotzar, G. M., Davy, D. T., Berilla, J., and Goldberg, V. M.: Torsional loads in the early postoperative period following total hip replacement. J Orthop Res. 13:945-955, 1995.

77. Kotzar, G. M., Davy, D. T., Goldberg, V. M., Heiple, K. G., Berilla, J., Heiple, K. G. J., Brown, R. H., and Burstein, A. H.: Telemeterized in vivo hip joint force data: a report on two patients after total hip surgery. J Orthop Res. 9:621-633, 1991.

78. Kurtz, S. M., Muratoglu, O. K., Evans, M., and Edidin, A. A.: Advances in the processing, sterilization, and crosslinking of ultra- high molecular weight polyethylene for total joint arthroplasty [In Process Citation]. Biomaterials. 20:1659-1688, 1999.

79. Kurtz, S. M., Pruitt, L., Jewett, C. W., Crawford, R. P., Crane, D. J., and Edidin, A. A.: The yielding, plastic flow, and fracture behavior of ultra-high molecular weight polyethylene used in total joint replacements. Biomaterials. 19:1989-2003, 1998.

80. Kuster, M. S., Wood, G. A., Stachowiak, G. W., and Gachter, A.: Joint load considerations in total knee replacement. J Bone Joint Surg Br. 79:109-113, 1997.

81. Lee, D. C., Kim, D. H., Scott, R. D., and Suthers, K.: Intraoperative flexion against gravity as an indication of ultimate range of motion in individual cases after total knee arthroplasty. J Arthroplasty. 13:500-503, 1998.

82. Li, G., Kaufman, K. R., Chao, E. Y., and Rubash, H. E.: Prediction of antagonistic muscle forces using inverse dynamic optimization during flexion/extension of the knee. J Biomech Eng. 121:316-322, 1999.

83. Li, G., Kawamura, K., Barrance, P., Chao, E. Y., and Kaufman, K.: Prediction of muscle recruitment and its effect on joint reaction forces during knee exercises. Ann Biomed Eng. 26:725-733, 1998.

84. Lindstrand, A., Stenstrom, A., and Lewold, S.: Multicenter study of unicompartmental knee revision. PCA, Marmor, and St Georg compared in 3,777 cases of arthrosis. Acta Orthop Scand. 63:256-259, 1992.

85. Lu, T. W., O'Connor, J. J., Taylor, S. J., and Walker, P. S.: Validation of a lower limb model with in vivo femoral forces telemetered from two subjects. J Biomech. 31:63-69, 1998.

86. Lu, T. W., Taylor, S. J., O'Connor, J. J., and Walker, P. S.: Influence of muscle activity on the forces in the femur: an in vivo study. J Biomech. 30:1101-1106, 1997.

87. Lutz, G. E., Palmitier, R. A., An, K. N., and Chao, E. Y.: Comparison of tibiofemoral joint forces during open-kinetic-chain and closed-kinetic-chain exercises. J Bone Joint Surg Am. 75A:732-739, 1993.

88. Mahoney, O. M., McClung, C. D., dela Rosa, M. A., and Schmalzried, T. P.: The effect of total knee arthroplasty design on extensor mechanism function. J Arthroplasty. 17:416-421, 2002.

89. Maxian, T. A., Brown, T. D., Pedersen, D. R., and Callaghan, J. J.: A sliding-distance-coupled finite element formulation for polyethylene wear in total hip arthroplasty. J Biomech. 29:687-692, 1996.

90. McKellop, H. A., Shen, F. W., Campbell, P., and Ota, T.: Effect of molecular weight, calcium stearate, and sterilization methods on the wear of ultra high molecular weight polyethylene acetabular cups in a hip joint simulator. J Orthop Res. 17:329-339, 1999.

91. Messier, S. P.: Osteoarthritis of the knee and associated factors of age and obesity: effects on gait. Med Sci Sports Exerc. 26:1446-1452, 1994.

92. Mintz, L., Tsao, A. K., McCrae, C. R., Stulberg, S. D., and Wright, T.: The arthroscopic evaluation and characteristics of severe polyethylene wear in total knee arthroplasty. Clin Orthop Relat Res. 273:215-222, 1991.

93. Morris, B. A., D'Lima, D. D., Slamin, J. E., Kovacevic, N., Arms, S. W., Townsend, C., and Colwell, C. W., Jr.: e-Knee: Evolution of the electronic knee prosthesis: Telemetry technology development. J Bone Joint Surg Am. 83-A Suppl 2:62-66, 2001.

94. Morrison, J. B.: The mechanics of the knee joint in relation to normal walking. J Biomech. 3:51-61, 1970.

95. Nafei, A., Kristensen, O., Knudsen, H. M., Hvid, I., and Jensen, J.: Survivorship analysis of cemented total condylar knee arthroplasty. A long-term follow-up report on 348 cases. J Arthroplasty. 11:7-10, 1996.

96. Nagamine, R., White, S. E., McCarthy, D. S., and Whiteside, L. A.: Effect of rotational malposition of the femoral component on knee stability kinematics after total knee arthroplasty. J Arthroplasty. 10:265-270, 1995.

97. Nagura, T., Dyrby, C. O., Alexander, E. J., and Andriacchi, T. P.: Mechanical loads at the knee joint during deep flexion. J Orthop Res. 20:881-886, 2002.

98. National Center of Health Statistics. National Center for Health Statistics. 1992.

99. National Hospital Discharge Surveys. National Hospital Discharge Surveys. 1993.

100. Nisell, R., Ericson, M. O., Nemeth, G., and Ekholm, J.: Tibiofemoral joint forces during isokinetic knee extension. Am J Sports Med. 17:49-54, 1989.

101. Nissan, M. The use of permutation approach in the solution of joint biomechanics: the knee. Engineering in medicine. 10, 39-43. 1981.

102. Pedersen, D. R., Brand, R. A., Cheng, C., and Arora, J. S.: Direct comparison of muscle force predictions using linear and nonlinear programming. J Biomech Eng. 109:192-199, 1987.

103. Perry, J., Antonelli, D., and Ford, W.: Analysis of knee-joint forces during flexed-knee stance. J Bone Joint Surg Am. 57:961-967, 1975.

104. Peters, P. C. J., Engh, G. A., Dwyer, K. A., and Vinh, T. N.: Osteolysis after total knee arthroplasty without cement. J Bone Joint Surg Am. 74A:864-876, 1992.

105. Petersilge, W. J., Oishi, C. S., Kaufman, K. R., Irby, S. E., and Colwell Jr, C. W.: The effect of trochlear design on patellofemoral shear and compressive forces in total knee arthroplasty. Clin Orthop Relat Res. 309:124-130, 1994.

106. Peterson, C. D., Hillberry, B. M., and Heck, D. A.: Component wear of total knee prostheses using Ti-6A1-4V, titanium nitride coated Ti-6A1-4V, and cobalt-chromium-molybdenum femoral components. J Biomed Mater Res. 22:887-903, 1988.

107. Polyzoides, A. J., Dendrinos, G. K., and Tsakonas, H.: The Rotaglide total knee arthroplasty. Prosthesis design and early results. J Arthroplasty. 11:453-459, 1996.

108. Postak, P. D., Heim, C. S., and Greenwald, A. S.: Tibial plateau surface stress in TKA: a factor influencing polymer failure. J Am Acad Orthop Surg. 1994.

109. Rand, J. A. and Bryan, R. S.: Revision after total knee arthroplasty. Orthop Clin North Am. 13:201-212, 1982.

110. Ritter, M. A., Harty, L. D., Davis, K. E., Meding, J. B., and Berend, M. E.: Predicting range of motion after total knee arthroplasty. Clustering, log-linear regression, and regression tree analysis. J Bone Joint Surg Am. 85-A:1278-1285, 2003.

111. Rodosky, M. W., Andriacchi, T. P., and Andersson, G. B.: The influence of chair height on lower limb mechanics during rising. J Orthop Res. 7:266-271, 1989.

112. Rodricks, D. J., Patil, S., Pulido, P., and Colwell, C. W., Jr.: Press-fit condylar design total knee arthroplasty. Fourteen to seventeen-year follow-up. J Bone Joint Surg Am. 89:89-95, 2007.

113. Rohlmann, A., Bergmann, G., Graichen, F., and Mayer, H. M.: Telemeterized load measurement using instrumented spinal internal fixators in a patient with degenerative instability. Spine. 20:2683-2689, 1995.

114. Rostoker, W. and Galante, J. O.: Contact pressure dependence of wear rates of ultra high molecular weight polyethylene. J Biomed Mater Res. 13:957-964, 1979.

115. Rydell, N. W.: Forces acting on the femoral head-prosthesis. A study on strain gauge supplied prostheses in living persons. Acta Orthop Scand. 37:Suppl 88:1-132:5-61, 1966.

116. Sathasivam, S. and Walker, P. S.: Computer model to predict subsurface damage in tibial inserts of total knees. J Orthop Res. 16:564-571, 1998.

117. Schmidt, R. H.: Osteolysis: new polymers and new solutions. Orthopedics. 17:817-818, 1994.

118. Seireg, A. and Arvikar: The prediction of muscular load sharing and joint forces in the lower extremities during walking. J Biomech. 8:89-102, 1975.

119. Seireg, A. and Arvikar, R. J.: A mathematical model for evaluation of forces in lower extremities of the musculo-skeletal system. J Biomech. 6:313-326, 1973.

120. Sharkey, P. F., Hozack, W. J., Rothman, R. H., Shastri, S., and Jacoby, S. M.: Insall Award paper. Why are total knee arthroplasties failing today? Clin Orthop Relat Res. 404:7-13, 2002.

121. Singerman, R., Berilla, J., Archdeacon, M., and Peyser, A.: In vitro forces in the normal and cruciate-deficient knee during simulated squatting motion. J Biomech Eng. 121:234-242, 1999.

122. Singerman, R., Dean, J. C., Pagan, H. D., and Goldberg, V. M.: Decreased posterior tibial slope increases strain in the posterior cruciate ligament following total knee arthroplasty. J Arthroplasty. 11:99-103, 1996.

123. Su, F. C., Lai, K. A., and Hong, W. H.: Rising from chair after total knee arthroplasty. Clin Biomech (Bristol, Avon). 13:176-181, 1998.

124. Syed, I. Y. and Davis, B. L.: Obesity and osteoarthritis of the knee: hypotheses concerning the relationship between ground reaction forces and quadriceps fatigue in long-duration walking. Med Hypotheses. 54:182-185, 2000.

125. Szivek, J. A., Anderson, P. L., and Benjamin, J. B.: Average and peak contact stress distribution evaluation of total knee arthroplasties. J Arthroplasty. 11:952-963, 1996.

126. Taylor, S. J., Perry, J. S., Meswania, J. M., Donaldson, N., Walker, P. S., and Cannon, S. R.: Telemetry of forces from proximal femoral replacements and relevance to fixation. J Biomech. 30:225-234, 1997.

127. Taylor, S. J., Walker, P. S., Perry, J. S., Cannon, S. R., and Woledge, R.: The forces in the distal femur and the knee during walking and other activities measured by telemetry. J Arthroplasty. 13:428-437, 1998.

128. Taylor, W. R., Heller, M. O., Bergmann, G., and Duda, G. N.: Tibio-femoral loading during human gait and stair climbing. J Orthop Res. 22:625-632, 2004.

129. Thambyah, A., Goh, J. C., and De, S. D.: Contact stresses in the knee joint in deep flexion. Med Eng Phys. 27:329-335, 2005.

130. Tsakonas, A. C. and Polyzoides, A. J.: Reduction of polyethylene in a congruent meniscal knee prosthesis. Experimental and clinical studies. Acta Orthop Scand. Suppl 275:127-131, 1997.

131. Tsao, A., Mintz, L., McRae, C. R., Stulberg, S. D., and Wright, T.: Failure of the porous-coated anatomic prosthesis in total knee arthroplasty due to severe polyethylene wear [see comments]. J Bone Joint Surg Am. 75A:19-26, 1993.

132. US Bureau of the Census. US Bureau of the Census, Current Population Reports, Series P25-1130. 1994.

133. Wasielewski, R. C., Galante, J. O., Leighty, R. M., Natarajan, R. N., and Rosenberg, A. G.: Wear patterns on retrieved polyethylene tibial inserts and their relationship to technical considerations during total knee arthroplasty. Clin Orthop Relat Res. 299:31-43, 1994.

134. Weightman, B. and Light, D.: A comparison of RCH 1000 and Hi Fax 1900 ultrahigh molecular weight polyethylenes. Biomaterials. 6:177-183, 1985.

135. Weiner, D. K., Long, R., Hughes, M. A., Chandler, J., and Studenski, S.: When older adults face the chair-rise challenge. A study of chair height availability and height-modified chair-rise performance in the elderly. J Am Geriatr. Soc. 41:6-10, 1993.

136. Weir, D. J., Moran, C. G., and Pinder, I. M.: Kinematic condylar total knee arthroplasty. 14-year survivorship analysis of 208 consecutive cases. J Bone Joint Surg Br. 78:907-911, 1996.

137. Whiteside, L. A.: Cementless total knee replacement. Nine- to 11-year results and 10-year survivorship analysis. Clin Orthop Relat Res. 309:185-192, 1994.

138. Wilk, K. E., Escamilla, R. F., Fleisig, G. S., Barrentine, S. W., Andrews, J. R., and Boyd, M. L.: A comparison of tibiofemoral joint forces and electromyographic activity during open and closed kinetic chain exercises. Am J Sports Med. 24:518-527, 1996.

139. Wilke, H. J., Neef, P., Caimi, M., Hoogland, T., and Claes, L. E.: New in vivo measurements of pressures in the intervertebral disc in daily life. Spine. 24:755-762, 1999.

140. Williams, I. R., Mayor, M. B., and Collier, J. P.: The impact of sterilization method on wear in knee arthroplasty. Clin Orthop Relat Res.170-180, 1998.

141. Yashar, A. A., D'Lima, D. D., Irby, S. E., Kaufman, K. R., and Colwell, C. W., Jr.: The effect of mobile bearing knee replacement on 3 dimensional kinematics. ORS. 43:262, 1997.